Title: A multiomics analysis of direct interkingdom dynamics between influenza A virus and *Streptococcus pneumoniae* uncovers host-independent changes to bacterial virulence fitness

Authors: Maryann P. Platt[1], Yi-Han Lin[1], Trevor Penix[2], Rosana Wiscovitch-Russo[1], Isha Vashee[1], Chris A. Mares[3], Jason W. Rosch[2], Yanbao Yu[1,4], Norberto Gonzalez-Juarbe[1]*

Affiliations: [1]Infectious Diseases and Genomic Medicine Group, J Craig Venter Institute, 9605 Medical Center Drive Suite 150, Rockville, MD, USA. [2]Department of Infectious Diseases, St. Jude Children's Research Hospital, Memphis, TN, USA. [3]Department of Life Sciences, Texas A&M University-San Antonio, SA, USA. [4]Department of Chemistry and Biochemistry, University of Delaware, Newark, DE, USA.

***Corresponding Author:**

Norberto Gonzalez-Juarbe

9605 Medical Center Drive Suite 150

Rockville, MD 20850

ngonzale@jcvi.org

Abstract

Background: For almost a century, it has been recognized that influenza A virus (IAV) infection can promote the development of secondary bacterial infections (SBI) mainly caused by *Streptococcus pneumoniae* (*Spn*). Recent observations have shown that IAV is able to directly bind to the surface of *Spn*. To gain a foundational understanding of how direct IAV-*Spn* interaction alters bacterial biological fitness we employed combinatorial multi-omic and molecular approaches.

Results: Here we show IAV significantly remodels the global transcriptome, proteome and phosphoproteome profiles of *Spn* independently of host effectors. We identified *Spn* surface proteins that interact with IAV proteins (hemagglutinin, nucleoprotein, and neuraminidase). In addition, IAV was found to directly modulate expression of *Spn* virulence determinants such as pneumococcal surface protein A, pneumolysin, and factors associated with antimicrobial resistance among many others. Metabolic pathways were significantly altered leading to changes in *Spn* growth rate. IAV was also found to drive *Spn* capsule shedding and the release of pneumococcal surface proteins. Released proteins were found to be involved in evasion of innate immune responses and actively reduced human complement hemolytic and opsonizing activity. IAV also led to phosphorylation changes in *Spn* proteins associated with metabolism and bacterial virulence. Validation of proteomic data showed significant changes in *Spn* galactose and glucose metabolism. Furthermore, supplementation with galactose rescued bacterial growth and promoted bacterial invasion, while glucose supplementation led to enhanced pneumolysin production and lung cell apoptosis.

Conclusions: Here we demonstrate that IAV can directly modulate *Spn* biology without the requirement of host effectors and support the notion that inter-kingdom interactions between human viruses and commensal pathobionts can promote bacterial pathogenesis and microbiome dysbiosis.

Introduction

During annual epidemics, influenza virus causes up to 3-5 million infections and results in hundreds of thousands of deaths worldwide[1]. Disease complications and the healthcare burden rises with the development of secondary bacterial infection (SBI), which results in aggravated illness and higher mortality[2]. The major example of such synergy was observed during the 1918 Flu pandemic, in which *Streptococcus pneumoniae* (*Spn*) was recovered in ~95% of all fatal cases. During the 2009 influenza A H1N1 pandemic, up to 43% of lung specimens recovered from fatal cases also had bacterial infection[3, 4]. SBIs are mainly caused by the Gram-positive bacterium, *Spn*[5, 6], the most common cause of community acquired pneumonia (CAP)[7]. *Spn* normally exists as a commensal in the human nasopharynx and is found in more than 95% of children under age 2, 40% of children under age 5[8] and up to 39% in the elderly[9]. Up to this point, most studies that characterize the lethal synergism between influenza A virus (IAV) and *Spn* mainly focus on the effect IAV infection has on the mammalian host. Major findings over the last decades are: 1) Factors enhancing bacterial adherence 2) Factors facilitating bacterial access to normally sterile sites, 3) Factors altering innate immune responses and 4) Synergism between viral and bacterial proteins to kill mammalian cells[5, 10-15]. During and after influenza infection, commensal bacteria can translocate from the upper to the lower respiratory tract and cause an exacerbated form of pneumonia[13, 16].

How direct physiological or pathogenic changes to bacteria are induced by direct human virus exposure in the absence of host mediated inflammatory mediators, has not been well described. *Spn* normally colonizes the nasopharynx asymptomatically. However, upon host infection with influenza virus, the bacterium can be triggered to disperse to the lungs and cause severe infection[8, 17]. Transcriptomics based studies have suggested that upon IAV infection, host antiviral inflammatory responses lead to differential expression of *Spn* genes promoting biofilm dispersal and translocation to the lungs[17]. In contrast, a recent report by Rowe *et al.*

69 studying the early stages of disease (prior to development of severe infection), showed that IAV
70 was able to bind directly to *Spn*, promoting adhesion, and increasing lethality in a mouse model
71 of acute infection[18]. This phenomenon (direct binding of human virus to bacteria) has only been
72 previously observed in studies of *Spn* interaction with respiratory syncytial virus (RSV) and
73 suggests that respiratory viruses could directly modulate colonizing bacteria at a molecular level
74 independently of host factors[19, 20]. However, the underlying molecular mechanisms for these
75 phenomena have not been explored to date.

76 In this study, we investigate direct IAV-*Spn* interactions with emphasis on how the virus
77 causes a switch in *Spn* physiology and virulence fitness without the requirement of host signals.
78 Here we use Mass Spectrometry-based and molecular approaches to provide unique details of
79 the changes occurring at the global protein level, as well as changes in phosphorylation patterns,
80 protein secretion (secretome), growth and virulence after *Spn* exposure to IAV in a host
81 independent manner.

82

83 ## Results

84 **Influenza A virus modulates *Spn* growth and capsule production.** Here we designed a model
85 in which IAV is incubated with planktonic *Spn* (strain TIGR4) in liquid culture. A reduction in *Spn*
86 growth was observed when incubated with IAV at a 1:1 ratio, with no changes in growth rate
87 observed after *Spn* incubation with heat killed IAV (**Fig. 1A**). A similar effect was observed when
88 *Spn* strains WU2, 6A10 and D39[21] (**Fig. S1**) or additional pathogens *Escherichia coli* and
89 *Pseudomonas aeruginosa*[22] were co-incubated with IAV, but was not observed in the
90 nosocomial pathogen *Serratia marcescens*[23] (**Fig. S2**). When *Spn* is grown on agar plates, two
91 distinct colony morphologies can be observed under oblique transmitted light. These phenotypes

are named transparent (low capsule expression) and opaque (high capsule expression)[24]. After incubation with IAV, we observed a dose-dependent increase in the transparent phenotype of *Spn* (**Fig. 1B**). Importantly, when biofilm grown *Spn* was challenged with IAV, a significant increase in dispersal was observed, suggesting that IAV promotes a switch from biofilm to planktonic phenotype (**Fig. 1C**). These observations suggest that *Spn* metabolism and capsule production are altered upon exposure to IAV. Of note, we tested viral stocks derived from embryonated eggs and tissue culture, and no stock-specific difference was seen in the observed phenotype (**Figure 1A**, **Fig. S3A**). We identified non-bacterial proteins present in the experimental media by label free-quantitative proteomics, which were mammalian, yeast, or influenza proteins mainly associated with tissue culture or bacterial culture media (**Fig. S3B**).

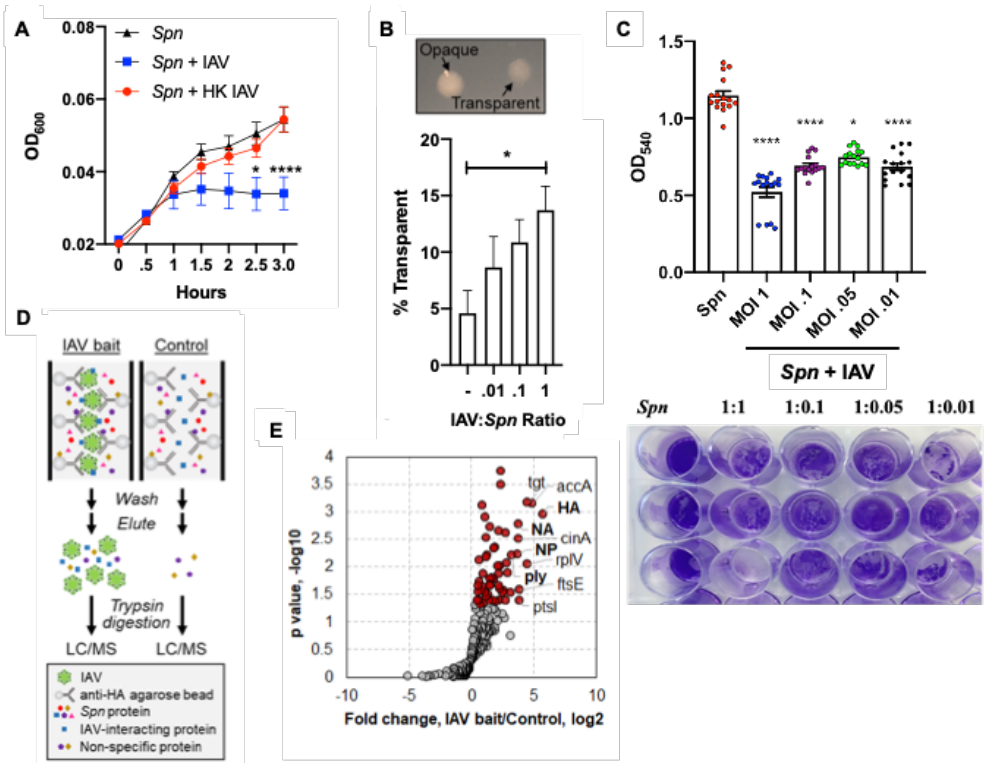

Figure 1. IAV-induced growth and morphological changes in *Spn*. (**A**) Growth of *Spn* strain TIGR4 in liquid media with/without IAV or with heat killed IAV (HK IAV). Data points represent mean ± SD. (**B**) Morphology of *Spn* colonies (upper panel) and counts on agar plates (lower

panel) in the presence or absence of IAV. Data points represent mean ± SEM from three separate experiments. (**C**) Static biofilm of *Spn* on a polystyrene plate was dispersed upon 24h incubation with IAV. *Spn* was stained by crystal violet. Quantitation was done by measure of absorbance at 540nm. (**D**) Schematic illustration of the experimental process for Affinity Enrichment Mass Spectrometry (AE-MS). Influenza virus particles were bound to HA antibody immobilized on agarose beads, which serve as bait to enrich *Spn* proteins. The control experiment did not contain the IAV bait. (**E**) Volcano plot showing proteins identified in the AE-MS analysis. Proteins significantly enriched in the presence of IAV bait (Student's t-test, $p<0.05$) are shown in red. IAV proteins are in bold. Kruskal-Wallis test with Dunn's multiple-comparison post-test. Asterisks denote the level of significance observed: * = $p \leq 0.05$; ** = $p \leq 0.01$; *** = $p \leq 0.001$.

Proteins as mediators of IAV-*Spn* interaction. Previous work by Rowe *et al.* showed direct interaction between *Spn* and IAV independent of both the glycosylation status of the virus and sialyation on the surface of *Spn*[18]. These data suggest that surface proteins could mediate the observed *Spn*-IAV interaction. Therefore, we used the Affinity Enrichment Mass Spectrometry (AE-MS) approach[25]to search for putative IAV-interacting *Spn* proteins, (**Fig. 1D**). IAV particles mixed with anti-Hemagglutinin (HA) agarose beads were incubated with *Spn* cell lysate. *Spn* proteins that can bind to the virus particles are retained on the beads. After extensive washes, proteins were eluted and analyzed by LC-MS. To exclude *Spn* proteins that bind non-specifically to the beads and resulted in background identification, we performed a control experiment without the addition of IAV particles to the antibody coated beads. Each experiment was performed in triplicate and protein quantitation was performed using the label-free quantitation (LFQ) approach.

Both the control and experimental group comprise of 200-300 quantifiable proteins, suggesting high background from non-specific interactions of *Spn* proteins to anti-HA beads. IAV

proteins, Hemagglutinin (HA), Neuraminidase (NA), and Nucleoprotein (NP), were confidently identified in the experimental group but not in the control group, indicating successful coating of anti-HA beads with IAV particles. After statistical analysis (Student's t-test, $p < 0.05$), 53 *Spn* proteins were found to be significantly enriched in the experimental group (i.e., with IAV particles) (**Fig. 1E, Spreadsheet S1**), 42 of which were increased by more than 2-fold. Of interest, one of the enriched proteins was pneumolysin (Ply) (increased by nearly 3-fold, **Fig. 1E**). Ply is a cholesterol-dependent pore-forming toxin that forms lytic pores on target membranes and modulates host inflammatory responses during *Spn* infection[26, 27]. Ply is known to be released by *Spn* upon autolysis and associate with host membranes via interaction with cholesterol[28]. Here, Ply from the cytosol may have been released upon *Spn* lysis to bind to IAV. However, a previous study indicated that Ply can localize to the *Spn* cell wall in a non-autolytic way, providing a mechanism for meaningful *Spn*-IAV interaction via Ply[29]. Other proteins found to bind influenza, and that are found in *Spn*'s cell or cell surface accessible include gapN, ptsI, accA, ftsE and cinA, among others (**Fig. 1E, Spreadsheet S1**). Our AE-MS approach identified candidate *Spn* proteins mediating the *Spn*-IAV interaction, and the downstream molecular mechanisms of the interactions between proteins need to be further studied in detail.

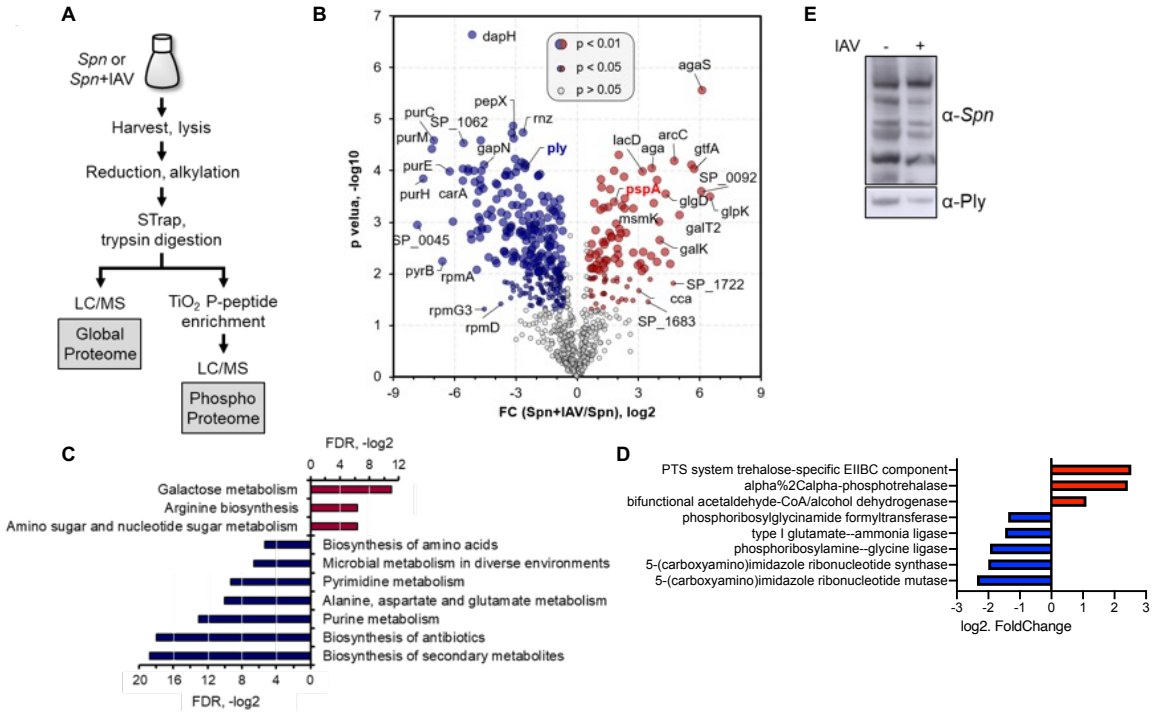

Figure 2. Global proteomic change of *Spn* in the presence of Influenza virus. (**A**) Workflow for global and phosphoproteome profiling of *Spn*. (**B**) *Spn* proteins identified from the global proteome analysis shown in a volcano plot. Red and blue are proteins significantly up- or down-regulated by 1.5-fold when co-incubated with IAV (Student's t-test, $p<0.05$ or $p<0.01$ for sizes indicated). KEGG enrichment analysis of significant (**C**) proteins and (**D**) transcripts. (**E**) Western blot of *Spn* lysate grown in presence or absence of IAV, probed with a polyclonal anti-*Spn* or anti-Pneumolysin antibody.

Proteome profile of *S. pneumoniae* is directly altered by influenza A virus. To gain a better understanding of the molecular changes to *Spn* upon direct interaction with IAV, we profiled the global *Spn* proteome with and without co-culture with IAV for 1 hour at a 1:1 ratio. The cell pellets (each in biological triplicates) were processed following the Suspension Trapping (STrap) approach with in-house assembled filter devices[30]. The resulting peptides were subjected to

direct liquid chromatography–tandem mass spectrometry (LC-MS/MS) analysis for global proteomics, or titanium dioxide (TiO_2) based phosphopeptide enrichment and then LC-MS/MS analysis for phosphoproteomics (**Fig. 2A**). The MaxLFQ based label-free quantitation (LFQ) was performed to determine proteome-level changes in response to IAV challenge[31]. Overall, 937 *Spn* proteins were quantified (≤ 1% FDR on both protein and peptide level), comparable to the quantifiable *Spn* proteome size of 919 proteins reported by a recent study[32]. In another independent set of experiments, we identified 1,036 quantifiable proteins, with 85% of them commonly quantified, indicating good experimental reproducibility (**Fig. S4A**). The overall proteome spanned around five orders of magnitude (**Fig. S4B**). Correlation between the biological replicates was high (Pearson $r = 0.97 \pm 0.01$; n = 6. **Fig. S3C**), whereas the inter-group correlation was low (0.75 ± 0.02; n = 9). The data implied that the IAV challenge-dependent proteome-level alternations could be captured by our approach, thereby suggesting its general applicability for quantitative proteomics. Of the quantifiable *Spn* proteins (in at least 2 of 3 replicates), 378 of them showed a significant difference between the two groups (Student's t-test, $p < 0.05$), including 104 and 274 proteins up- and down-regulated (fold change ≥ 1.5) in the presence of IAV, respectively (**Fig. 2B**, **Spreadsheet S2**). Their differential expressions were also verified in the second set of experiments (**Fig. S4D**). This finding provides the first global view of how IAV alters the *Spn* proteome, showing that one-third of quantifiable proteins had altered expression. Kyoto Encyclopedia of Genes and Genomes (KEGG) pathway enrichment analysis showed that approximately one third of the significant proteins are involved in metabolic pathways (FDR = 9.30E-13) (**Fig. 2C**), suggesting IAV directly influences *Spn* metabolism. Proteins associated with carbohydrate, amino acid, and nucleotide metabolism pathways were downregulated in the presence of IAV (**Fig. 2C**), consistent with the slower growth phenotype (**Fig. 1A**). Purine and pyrimidine synthesis are central to many metabolic processes of *Spn*[33], including DNA synthesis and capsule production[34, 35]. Our proteomic analysis showed 9 of the purine biosynthesis enzymes (PurB, PurC, PurD, PurE, PurF, PurH, PurK, PurM, and PurN) and 11 of

the pyrimidine biosynthesis proteins (CarA, CarB, PyrB, PyrC, PyrDA, PyrDB, PyrE, PyrF, PyrH, PyrK, and PyrR) were down-regulated upon IAV challenge (**Fig. S5 and Fig. S6**), many of them by more than 10-fold. These observations directly correlated to early transcriptional changes observed after incubation of *Spn* with IAV (**Fig. 2D**, **Spreadsheet S3**). Moreover, proteins associated with amino acid biosynthesis pathways (**Fig. S7**) and transport of amino acids (e.g., AliA, AliB, AmiE, AmiF) were also downregulated in the presence of IAV. Among the significantly down-regulated proteins, we also found several capsule synthesis proteins, including CpsE, CpsF, CpsG, and CpsK[36] (**Fig. S8**), indicating reduced capsule production and consistent with our observation that more transparent colonies were present on agar plates after *Spn* co-culture with IAV (**Fig. 1B**). In contrast, proteins that control cell division, including FtsA, ABC transporters FtsE, FtsX, and DivIB[37-39], were found up-regulated (**Fig. S8**).

Regulation of carbohydrate metabolism has been indicated to directly coordinate pneumococcal colonization and virulence[40]. We found that catabolite control protein A (CcpA), a regulator for carbohydrate utilization of *Spn*[41-43], was slightly up-regulated (1.8-fold) in the presence of IAV (**Fig. S8**), but glycolysis, the pathway *Spn* utilizes for glucose metabolism, was mainly down-regulated (**Fig. S9**). Importantly, galactose metabolism, which occurs preferentially in *Spn* that colonizes the respiratory tract[40] and cardiac tissues[44, 45] to modulate virulence, was found to be enriched among up-regulated proteins (**Fig. 2C**, **Fig. S10**). Enzymes involved in galactose metabolism pathways, the Leloir pathway (e.g. Aga, GalK, GalT2) and the tagatose 6-phosphate pathway (e.g. LacA, LacB, LacC, LacD)[46, 47], were found to be up-regulated. The complete list of proteins significantly altered in the presence of IAV can be found in **Spreadsheet S2.** Together, the change in utilization of sugars upon IAV challenge indicates not only altered metabolism, but also a potential virulence switch in *Spn*.

Supporting our virulence switch hypothesis, several virulence proteins were also found to be differentially expressed when *Spn* was challenged with IAV. The pneumococcal surface protein

A (PspA), a surface-exposed virulence molecule of *Spn* that helps subvert the host innate immune response by interfering with the complement system[26, 48], was found to be almost 2-fold up-regulated in the presence of IAV (**Fig. 2B**). In contrast, Ply was found to be more than 5-fold down-regulated (**Fig. 2B**) in the presence of IAV. The reduction in Ply was further validated by immunoblot (**Fig. 2E**). Of note, of ten common proteins associated with antimicrobial resistance[49], five were found to significantly change upon IAV incubation. Downregulated factors were murD, murG, metG and rpoB, whereas murI was observed upregulated. While expression of the serine/threonine kinase StkP did not change (**Fig. S5**) its phosphorylation was significantly changed in multiple sites (**Fig. 3**), suggesting its enhanced activity. The intricate regulation of virulence factor expression upon IAV co-incubation reflects how *Spn* virulence can be modulated. Despite the change of several pathways and *Spn* virulence determinants, IAV challenge did not change expression of the energy-coupling factor transporter ATP-binding protein EcfA2 (also known as SP_2220 or CbiO2), a putative cobalt transporter which when absent has been reported to be involved in enhanced pneumococcal pathogenicity in IAV-infected animals[50]. Finally, even in the presence of IAV, there was very low expression (quantified by ≤ 3 peptides) of the oxalate/formate antiporter SP_1587, which has been shown to regulate bacteremia, neutrophil infiltration, and pulmonary damage in IAV-infected mice[51]. This might reflect a need for interaction with the host (in addition to viral proteins) to alter expression of other virulence factors and colonize the lungs without induction of excess inflammation. In summary, our global proteomic analyses substantiate our initial observations that *Spn* growth, metabolism, and virulence, are directly affected upon exposure to IAV.

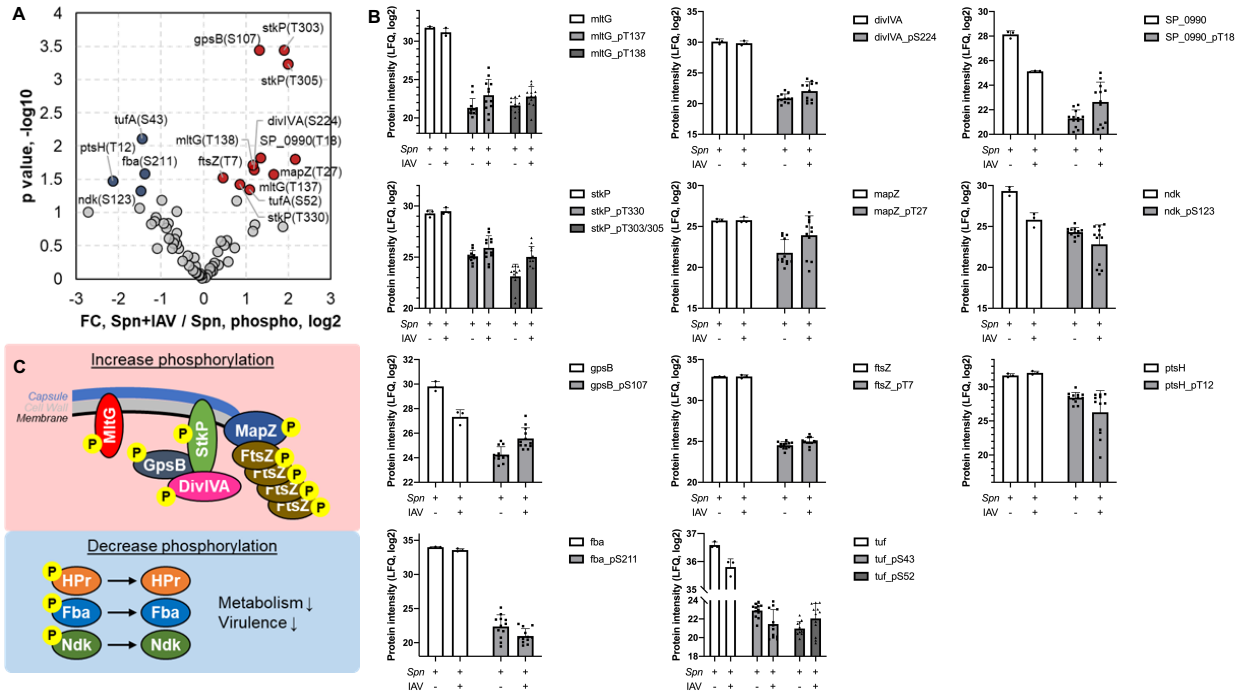

Figure 3. Change in *Spn* phosphoproteome in the presence of Influenza virus. (**A**) Volcano plot showing fold changes of phosphopeptides vs their p-values. Significantly changed phosphopeptides are shown in red (up-regulated) and blue (down-regulated) in the presence of IAV (Student's t-test p<0.05). (**B**) Peptide counts of the unmodified (white) and phosphorylated (gray) forms of indicated proteins in the absence or presence of IAV. Data reflect mean ± SD. (**C**) The top scheme shows the proteins with increased phosphorylation, most of which are known to localize to the septum during cell division. The bottom blue square shows proteins that are downregulated in phosphorylation, and their related functions.

IAV directly alters *Spn* protein phosphorylation. Phosphorylation is an important post-translational protein modification that regulates many cellular processes across all kingdoms of life[52]. In bacteria, two-component systems mediate cellular responses to environmental cues via histidine phosphorylation, while serine/threonine and tyrosine kinases also exist to modulate various cellular functions[53, 54]. In *Spn*, there is one serine/threonine kinase, StkP, and one

tyrosine kinase, CpsD, identified as regulators of cell wall synthesis, cell division, and capsule synthesis[53, 55]. To further elucidate the molecular and functional changes in *Spn* upon its direct interaction with IAV, we analyzed the phosphoproteome of *Spn* after IAV challenge using a TiO_2-based phosphopeptide enrichment method[56, 57] (**Fig. 2A**). Collectively, we quantified 108 class-1 phosphopeptides (probability score > 0.75)[58] derived from 55 *Spn* proteins, similar to the size of a previously reported *Spn* phosphoproteome[59]. We further required that quantifiable phosphopeptides appear in at least two out of three replicates of each group, resulting in 66 phosphopeptides from 29 *Spn* proteins (**Fig. 3A, Spreadsheet S4**). Among them, 16 were serine phosphorylation, 33 were threonine, and 17 were tyrosine phosphorylation. Both StkP and CpsD were identified in our phosphoproteome analysis with multiple phosphorylation sites. For StkP, 5 threonine residues located in the juxta-membrane region (Thr293, Thr295, Thr303, Thr305, Thr330)[53, 60] were identified, whereas in CpsD, 4 tyrosine residues (Tyr215, Tyr218, Tyr221, Tyr224) and 1 serine residue (Ser220) located in the C-terminal Y-rich domain[55, 61] were identified. Proteins that were previously found to be substrates of StkP, such as DivIVA, MapZ, and FtsZ[53, 62-64], were identified with multiple phosphorylation sites (**Table S1, Spreadsheet S4**). CpsE, a component within the capsular polysaccharide synthesis complex[55], and SP_1368, a membrane protein that contains a LytR_cpsA_psr domain, were identified with tyrosine phosphorylation, and therefore could be possible substrates of CpsD. Some phosphoproteins we identified are involved in metabolic pathways, such as Fba, Gap, GpmA (glycolysis), Ndk and NrdE (purine synthesis) (**Fig. 3A**). Additionally, other identified *Spn* phosphoproteins have never been reported before (**Table S1**). Identified phosphoproteins are involved in cell growth, capsule synthesis, and metabolism[59, 64] and were differentially modified upon *Spn* interaction with IAV.

Further analysis of the *Spn* phosphoproteome after challenge with IAV. 15 phosphopeptides were found to be significantly different between the two groups (Student's t-test, $p<0.05$, **Fig. 3A**).

StkP and several of its substrates, including MapZ, DivIVA, MltG, GpsB, and FtsZ, were found to be upregulated in phosphorylation when IAV was present (**Fig. 3A, B, Table S1**). MapZ directs the FtsZ (Z-ring) assembly and constriction during cell division, while StkP arrives in the mid-cell later where it phosphorylates DivIVA and decreases peripheral peptidoglycan synthesis[53, 62, 65]. GpsB mediates localization of StkP to the septum and is required for its kinase activity[62, 65, 66] (**Fig. 3C**). The abundance level of these proteins was not changed (**Fig. 3B, Spreadsheet S2**) except GpsB, which was found to be downregulated, indicating a true increase in phosphorylation of these proteins. The function of phosphorylation at specific sites in these proteins needs to be studied further. Proteins that were found to be downregulated in phosphorylation were mostly metabolic proteins (Fba, Ndk, PtsH) (**Fig. 3B**). Notably, the phosphocarrier protein Hpr (PtsH), had the largest decrease in phosphorylation, at Thr12, by more than 4-fold. The phosphorylation of Hpr has been shown to mediate CcpA interaction with genes that regulate carbohydrate usage and virulence factor expression[41, 67]. Taken together, this is consistent with our observations in the global proteome and suggests a switch in metabolism and virulence when *Spn* is challenged with IAV (**Fig. 3C**).

The release of *Spn* surface proteins is increased upon challenge with influenza A virus promoting evasion of complement activity. Like many other bacteria, *Spn* has many surface proteins important for colonization, virulence, and host invasion[68, 69]. Some of these surface proteins bind to cell wall phosphorylcholine, some are lipoproteins that associate with membrane transporters, and some have unknown anchoring mechanisms. The observed reduction in *Spn* capsule production after challenge with IAV (**Fig. 1B**) may lead to the release of surface proteins. To address this hypothesis, we performed proteomic profiling of the conditioned media used to grow *Spn* which contains bacterial proteins released from the cell surface upon challenge with IAV (**Fig. 4A**). Collectively, 30 *Spn* proteins were identified in the conditioned media, most of which had higher abundance (by peptide-spectrum match (PSM) count) after IAV challenge

298 (**Spreadsheet S5**). Consistent with our hypothesis, this result suggests that IAV can trigger *Spn*
299 surface protein release, possibly due to reduced capsulation (**Fig. 1B**).

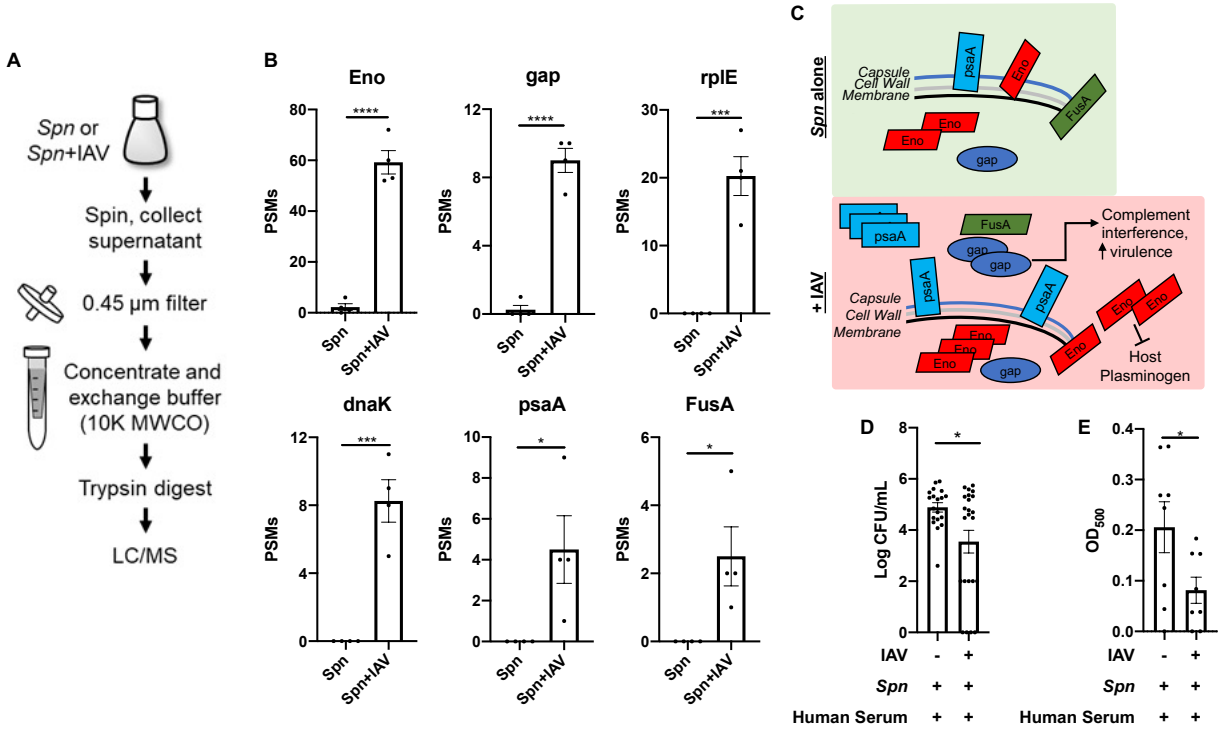

300

301 **Figure 4. Release of *Spn* surface proteins was increased in the presence of Influenza virus**
302 **and promotes complement inhibition.** (**A**) Workflow for the collection and processing of
303 extracellular *Spn* proteins for LC/MS analysis. (**B**) PSM count of extracellular *Spn* proteins in the
304 presence or absence of IAV (Data reflect n = 4 presented as mean ± SD, Two-tailed Student's t-
305 test, *p <0.05, ***p<0.001, ****p<0.0001). Eno, enolase; RplE, 50S ribosomal protein L5; GAP,
306 Glyceraldehyde-3-phosphate dehydrogenase; dnaK, Chaperone protein; PsaA, Manganese ABC
307 transporter substrate-binding lipoprotein; FusA, Elongation factor G. (**C**) Schematic model of the
308 proposed IAV-induced *Spn* pathway changes that lead to enhanced host invasion and inhibition
309 of complement. (**D**) Recovered *Spn* (CFU/ml) in phagocytosis assay. (**E**) Complement-driven
310 hemolysis assay in red blood cells challenged with *Spn* Δply. Student t test, asterisks denote the
311 level of significance observed: * = p ≤ 0.05; ** = p ≤ 0.01; *** = p ≤ 0.001.

312

313 Six proteins were found to be significantly increased in the conditioned media in the
314 presence of IAV (**Fig. 4B**), all of which are involved in either evasion of host responses or
315 modulation of bacterial virulence. Enolase and GAPDH are "moonlighting proteins," serving more
316 than one function in *Spn*[70]. In the cytosol they both function as glycolytic enzymes, however
317 when present at the *Spn* surface, even in low abundance[71], they bind and activate host
318 plasminogen increasing transmigration by degradation of the extracellular matrix[72-74]. In
319 addition, enolase and GAPDH both inhibit complement activation by binding to either C4b-binding
320 protein (C4BP)[75] or complement factor C1q[76], respectively. GAPDH binds to the complement
321 factor C1q[76]. Pneumococcal surface adhesin A (PsaA) is a lipoprotein and a component of the
322 membrane complex that transports manganese and zinc ions[77], and it is critical for *Spn*
323 virulence[78, 79]. FusA, an elongation factor that is surface-associated in *Streptococcus*
324 *oralis*[80], was significantly increased in the presence of IAV (**Fig. 4B**). Whether FusA is also a
325 surface protein in *Spn* and functions in complement interference[81] needs further investigation.
326 Overall, we found that IAV triggers the release of multiple *Spn* surface-associated proteins that
327 mediate host invasion and subversion of host immune response (**Fig. 4C**). To further support the
328 latter observation, we tested the ability of *Spn*'s condition media (after exposure to IAV) to
329 modulate complement activity. Treatment of WT *Spn* with conditioned media from *Spn* challenged
330 with IAV, we observed a decrease in phagocytosed bacteria by alveolar macrophages (MH-S)
331 (**Fig. 4D**). We then tested for changes in complement hemolytic activity induced by *Spn* released
332 proteins. Human serum was treated with concentrated conditioned media from an *Spn* deficient
333 in pneumolysin (i.e. Δ*ply,* with/without exposure to IAV, to avoid inducition of cell lysis by the pore-
334 forming activity of pneumolysin[82]), then serum was used to challenge sheep red blood cells.
335 We observed that conditioned media from Δ*ply* exposed to IAV reduced the hemolytic activity of

336 complement (**Fig. 4D**). Together, these results show that IAV can directly alter *Spn*'s ability to
337 counter the effects of innate immune effectors.

338

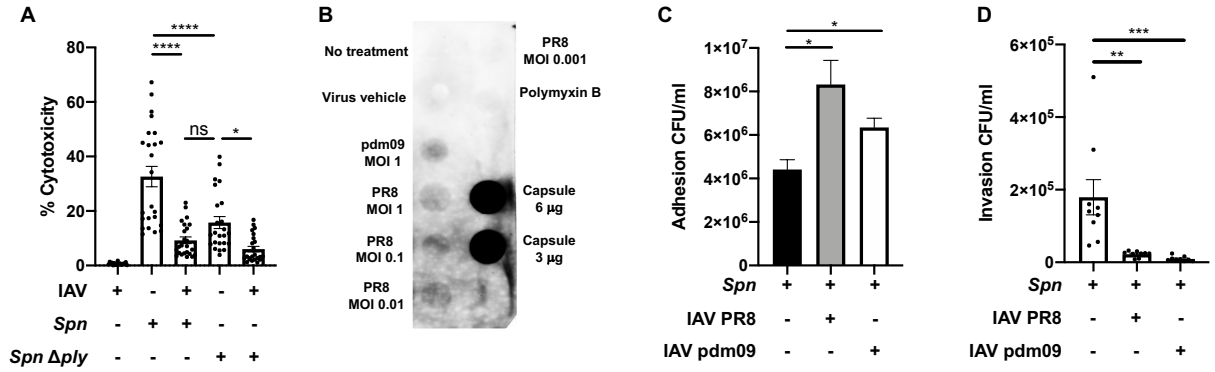

339

340 **Figure 5: Influenza influences *Spn*-induced cytotoxicity and adhesion and promotes**
341 **capsule shedding.** (**A**) *Spn* alone is significantly more toxic to A549 cells than *Spn* challenged
342 with IAV, or mutant *Spn* Δ*ply*, as measured by LDH cytotoxicity assay. IAV continues to synergize
343 with Δ*ply* to further reduce toxicity. Data reflects n=24 shown as mean ± SEM analyzed by one-
344 way ANOVA (*p<0.05, ****p<0.0001). (**B**) Dot blot of concentrated conditioned media from *Spn*
345 with or without IAV challenge using two viral strains, PR8 and H1N1 A/California/7/2009 (pdm09).
346 IAV challenge induced capsule release into media in a dose-dependent manner. Both IAV strains
347 induced *Spn* to increase adhesion (**C**) and decrease invasion (**D**) of A549 cells. Data in (**C**) and
348 (**D**) represent n=9 presented as mean ± SEM analyzed by Kruskal-Wallis test with Dunn's
349 multiple-comparison post-test. Asterisks denote the level of significance observed: * = $p \leq 0.05$;
350 ** = $p \leq 0.01$; *** = $p \leq 0.001$.

351

352 **IAV leads to changes in pneumococcus cytotoxicity, capsule shedding, and bacterial**
353 **adhesion though metabolic alterations.** Our proteomic data demonstrated that IAV challenge
354 led to decreased Ply expression in *Spn***.** To further test how IAV alters the virulence of *Spn*, we

first assessed how their interaction modulates *Spn*-induced toxicity in A549 type 2 respiratory epithelial cells. We observed that *Spn* challenged with IAV induced less cytotoxicity than an equivalent dose of *Spn* alone, comparable to that of a pneumolysin deficient mutant, Δ*ply* (**Fig. 5A**). These data further confirmed our previous results indicating reduced capsule production in *Spn* challenged with IAV (**Fig. 1B, Fig. S8**), we observed that IAV challenge induced capsule shedding in a dose dependent manner (**Fig. 5B**) and increased adhesion to A549 cells (**Fig. 5C**), in line with previous studies showing capsule shedding promotes host cell adhesion[83]. Increased adhesion was also observed in strains *Spn* D39, WU2 and 6A10 after bacterial incubation with IAV (**Fig. S11**). Interestingly, a significant reduction in cellular invasion was observed after *Spn* challenge with IAV (**Fig. 5D**). These results suggest that upon initial contact between *Spn* and IAV, the pneumococcus is primed towards an adhesion phenotype with low toxicity.

IAV-driven *Spn* glucose and galactose metabolism modulates growth and virulence strategies. After translocation from the nasopharynx to the lung, availability of sugars such as glucose and galactose is significantly increased[84-87]. Our multiproteomic studies showed that IAV induced changes to glucose and galactose metabolism (**Fig. 2, 3, Fig. S9, 10**). To test the effect of glucose and galactose availability in the biological changes induced by IAV in *Spn*, we supplemented 50% Todd Hewitt Broth with either glucose or galactose at 1% w/v. IAV-induced reduction in pneumococcal growth was rescued by galactose but not glucose (**Fig. 6A**). We observed an increase in pneumolysin expression (**Fig. 6B**), toxicity (**Fig. 6C**) and activation of apoptosis (**Fig. 6D**) after glucose but not with galactose supplementation. While no changes in adhesion were induced by either sugar (**Fig. 6E**), significantly increased invasion was observed upon galactose supplementation (**Fig. 6F**). These results suggest that IAV-induced changes to *Spn* upon initial contact, are further modulated by metabolite availability.

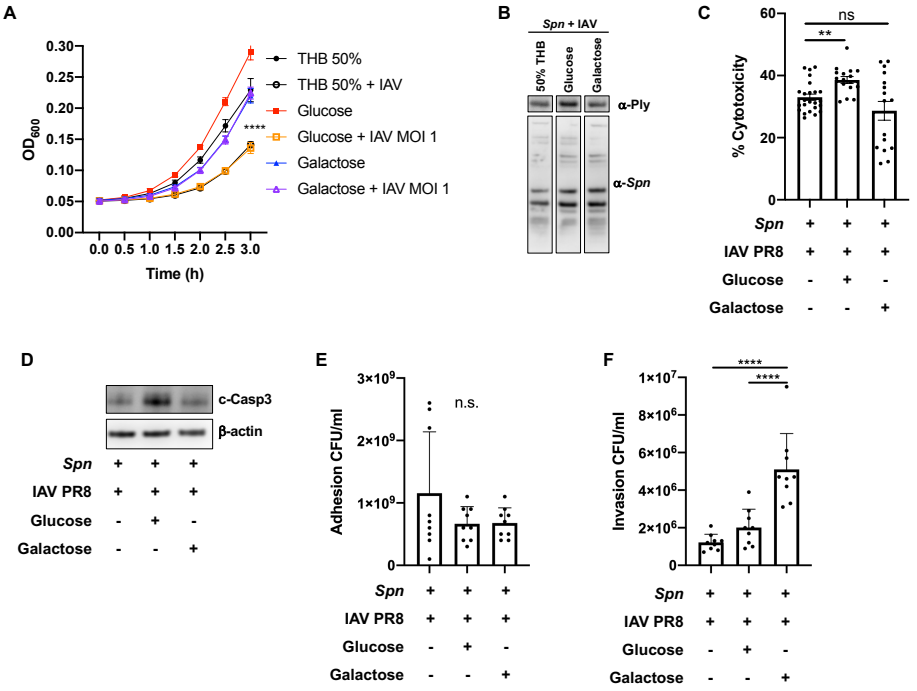

Figure 6: IAV-driven *S. pneumoniae* glucose and galactose metabolism modulates growth and virulence strategies. (**A**) Growth curves for Spn grown alone in minimal media (THB 50%, black closed circles), or supplemented with glucose 1% w/v (red solid squares) or galactose 1% w/v (blue solid triangles) do not differ significantly. Growth of *Spn* challenged with IAV was blunted when grown in minimal media (black open circles) or with glucose (orange open squares), but not with galactose (purple open triangles) Data reflect n=8 per condition (two-way ANOVA, ****p<0.0001 at t=3h). Glucose supplementation in media rescues (**B**) expression of pneumolysin as measured by Western blot, (**C**) exacerbated cytotoxicity to A549 cells as measured by LDH assay (n=8 per group, mean ± SEM, one-way ANOVA ****p<0.0001), and (**D**) cleaved caspase-3 expression by A549 cells infected with *Spn*+IAV. (**E**) Adhesion of bacteria to A549 cells was unchanged regardless of sugar supplementation, but *Spn*+IAV supplemented with galactose (**F**) improved invasion into A549 over *Spn* grown in glucose or un-supplemented media. Statistical analyses in **E** and **F** reflect n=9 per condition, mean ± SD, analyzed by Kruskal-Wallis test with Dunn's multiple-comparison post-test. Asterisks denote the level of significance observed: * = p ≤ 0.05; ** = p ≤ 0.01; *** = p ≤ 0.001.

Influenza virus infection of host respiratory epithelial cells leads to additional alterations to the pneumococcal proteome. Colonizing *Spn* has been shown to translocate from the nasopharynx to the lung and cause severe disease after establishment of IAV infection. To evaluate changes in the proteomic profile of *Spn* after exposure to IAV infected type II respiratory epithelial cells (RECs), we used an *in vitro* model of infection, which was previously shown to predispose RECs to bacterial toxin mediated necroptosis [15]. Herein, we infected A549 respiratory epithelial cells with IAV PR8 at an MOI of 2 [15]. Four hours post infection, cells were challenged with *Spn* at an MOI of 10 for an additional four hours. As controls *Spn* was grown in tissue culture media with or without IAV exposure for the duration of the experiment. A total of 369 proteins were expressed differentially ($P < 0.05$) (**Fig. 7A**). Principal Component Analysis (PCA) showed differential clustering of the bacterial proteins, suggesting each growth condition had an effect in pneumococcal biology (**Fig. 7B**). Hierarchical clustering revealed 3 distinct clusters of *Spn* proteins that changed expression between groups (**Spreadsheet S6**). Evaluation of the biological processes (GO terms) associated with cluster 1 differentially expressed proteins revealed mainly a decrease in proteins associated with cell wall biogenesis, nucleoside triphosphate biosynthetic process, peptidoglycan metabolic process, regulation of cell morphogenesis, and ion transport (cluster 1, **Fig. 7C**). In cluster 2, proteins showed increased expression only in the *Spn* isolated from the A549 cells that were previously infected with IAV. For these proteins GO terms associated with cell septum assembly, cytokinetic process, ATP biosynthetic process, and purine nucleoside triphosphate biosynthetic process (cluster 2, **Fig. 7C**). Lastly, proteins in cluster 3 revealed mainly an increase in proteins involved in 5-phosphoribose 1-diphosphate biosynthetic process, organophosphate metabolic process and tRNA aminoacylation, relative to unchallenged *Spn* control (cluster 3, **Fig. 7C**). Interestingly, *Spn*

420 proteins upregulated in the presence of the influenza infected host showed a shift in purine
421 metabolism, found decreased upon direct interaction between *Spn* and IAV.

422

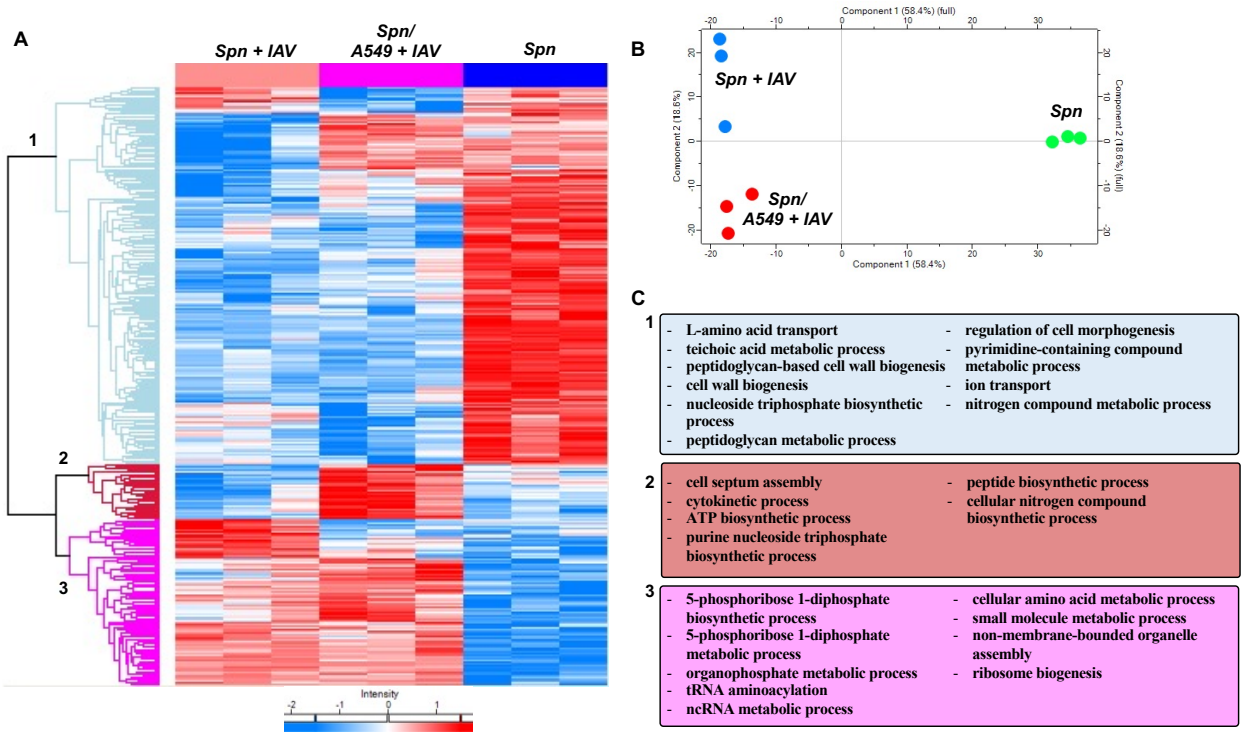

423

424 **Figure 7: Primary IAV infection of respiratory epithelial cells leads to additional alterations**
425 **to the pneumococcal proteome.** A549 respiratory epithelial cells were infected with IAV PR8 at
426 an MOI of 2. Four hours post infection, cells were challenged with *Spn* at an MOI of 10 for an
427 additional four hours. As controls *Spn* was grown in tissue culture media with or without IAV
428 exposure for the duration of the experiment. (**A**) Proteomic changes of *Spn* after IAV challenge,
429 in the presence of IAV infected A549 cells or mock challenge. Hierarchical clustering of label-free
430 quantification (LFQ) intensities of significantly changed proteins (ANOVA, P ,0.05) revealed 3
431 distinct clusters. Their abundance profiles among the groups were plotted in the heatmap (**A**). (**B**)
432 Principal component analysis denoting differences in *Spn* proteomic profiles. (**C**) Enriched GO
433 biological process terms are indicated for each marked cluster.

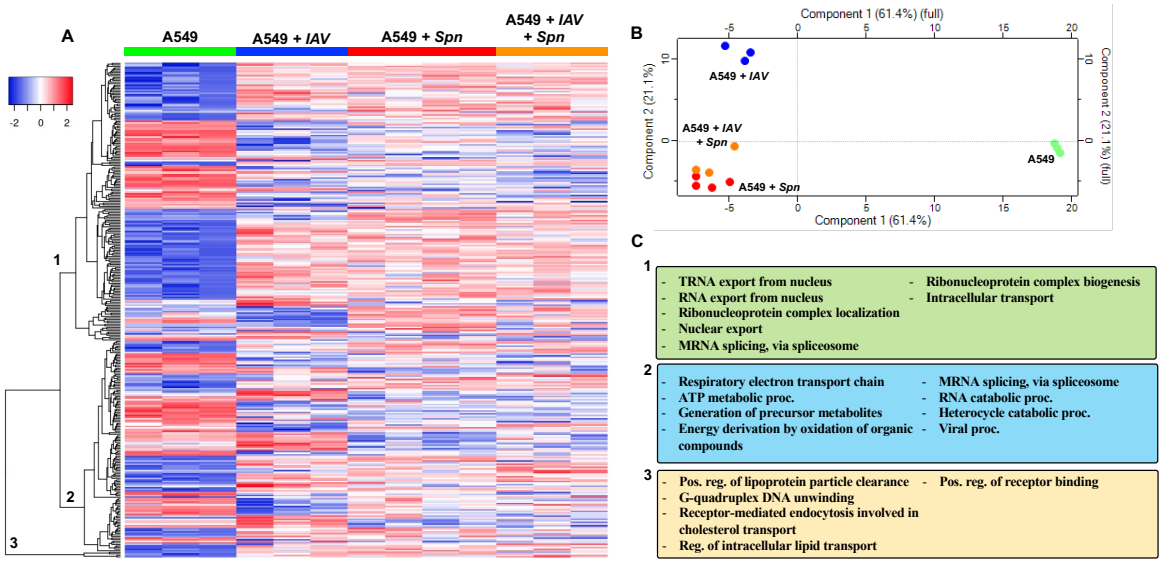

Figure 8: Sequential infection of RECs with IAV and *Spn* leads to differential proteomic remodeling. A549 respiratory epithelial cells were infected with IAV PR8 at an MOI of 2. Four hours post infection, cells were challenged with *Spn* at an MOI of 10 for an additional four hours. As control A549 was grown in tissue culture media exposure to any pathogen. Proteomic changes in A549 cells. (**A**) Hierarchical clustering of label-free quantification (LFQ) intensities of significantly changed proteins (ANOVA, P ,0.05) revealed 3 distinct clusters. Their abundance profiles among the groups were plotted in the heatmap. (**B**) Principal component analysis denoting differences in *Spn* proteomic profiles. (**C**) Enriched GO biological process terms are indicated for each marked cluster.

Sequential infection of RECs with IAV and *S. pneumoniae* leads to differential proteomic remodeling. Here we evaluated changes in the proteomic profile of RECs after sequential infection with IAV and *Spn* as previously described [15]. A549 cells were mock challenged or infected with IAV, *Spn* or sequentially infected with these pathogens. A total of 315 proteins were expressed differentially (P < 0.05) between the groups (**Fig. 8A**). Principal Component Analysis (PCA) showed that infected cells had significant proteome remodeling when compared to mock

(vehicle) infected cells (**Fig. 8B**). Hierarchical clustering revealed 3 distinct clusters of A549 proteins that changed expression between groups (**Spreadsheet S7**). Evaluation of the biological processes GO terms associated with cluster 1 differentially expressed proteins revealed in its majority an increase in proteins associated with RNA export from nucleus, ribonucleoprotein complex localization, peptidoglycan metabolic process, MRNA splicing, via spliceosome, and Intracellular transport (cluster 1, **Fig. 8C**). In cluster 2, proteins showed both increased and decreased expression, GO terms associated with these proteins were ATP metabolism, generation of precursor metabolites, energy derivation by oxidation of organic compounds, and viral processes (cluster 2, **Fig. 8C**). Lastly, proteins in cluster 3 mainly increased in expression and were found to be involved in receptor binding, lipoprotein clearance, and receptor-mediated endocytosis involved in cholesterol transport (cluster 3, **Fig. 8C**). These results suggest that viral and bacterial infections drive global changes to REC proteome, however upon sequential infection, the response is similar to the single bacterial infection group.

Discussion

Recent research has demonstrated direct interaction between nasopharyngeal commensal bacteria and IAV, causing a synergistic increase in susceptibility to bacterial infection and disease severity[88]. In this study, we define the biological alterations IAV induces upon direct interaction with *Spn.* We used the power of multi-proteomic approaches to reveal candidates for the underlying molecular interactions between *Spn* and IAV. Using AE-MS, we found *Spn* proteins that interact with IAV. Future experiments using other *Spn* mutants lacking putative IAV-interacting genes should be performed to validate candidate interaction partners in detail. Our experiments using *Spn* lacking the candidate IAV-interacting protein pneumolysin (Δ*ply*) demonstrated that IAV affects multiple molecular pathways in *Spn* (regarding host cytotoxicity), confirming data from our proteomic analyses. The combined global and phosphoproteome

476 analyses of *Spn* challenged with IAV revealed themes of altered metabolism, including glycolysis,
477 purine/pyrimidine synthesis, amino acid synthesis and a switch to galactose metabolism.
478 Galactose metabolism is an alternative energy production pathway that has been linked to *Spn*
479 virulence[44, 45]. Proteins that mediate cell division are more abundant (Fts proteins) or increased
480 in phosphorylation (StkP and substrates), suggesting a possible effort by the bacteria to modulate
481 cell growth without undergoing autolysis. Importantly, the slow growth of *Spn* early after contact
482 with IAV may be a way for bacteria released from the nasopharynx to prevent initial immune
483 activation and evade the effect of host antimicrobials while colonizing the respiratory tract[89-91].
484 It remains to be determined if, upon *in vivo* infection, these metabolic changes will lead to faster
485 growth due to the abundance of galactose in the respiratory tract[92]. This suggests IAV directly
486 primes *Spn* towards metabolic fitness to promote pulmonary infection.

487 The observed changes in the proteome and phosphoproteome suggested a possible
488 switch of gene expression towards an infectious phenotype. Also, the *Spn* biofilm dispersal
489 observed upon contact with IAV also support virulence switch as planktonic but not biofilm are
490 associated with pulmonary and invasive disease[93]. While the adhesion and immune evasion
491 factor PspA was up-regulated in the presence of IAV, IgA and Ply were down-regulated. It was
492 previously shown that mice challenged with pneumolysin have reduced influenza-associated
493 pathogenesis[94], which leads us to speculate that to counteract this effect, IAV may down-
494 regulate the production of Ply. PspA upregulation by IAV may also promote its binding to host
495 lactoferrin, potentiating iron acquisition and bacterial growth in the lower respiratory tract[95]. It
496 also indicates that IAV-mediated protein regulation may be under a more sophisticated spatial
497 and temporal control that fine tunes *Spn* virulence depending on the infection stage.

498 Capsule is known as an important virulence factor of *Spn* and is the basis for commercial
499 vaccines. While capsule is required for bacterial survival in the bloodstream (invasive
500 pneumococcal disease) and immune evasion[96], its reduction is not completely detrimental for

the bacterium's ability to cause respiratory disease[97] and cardiac damage[98]. Non-typeable *Spn* lacking capsule also exists and has been shown to be equally pathogenic[99]. Moreover, capsule shedding was recently described as a new pathway for the development of invasive disease[83]. We investigated whether IAV challenge alters the association of *Spn* surface proteins due to the observed reduction in capsule. Indeed, several *Spn* proteins, some previously known to be surface attached, were found to be increased extracellularly in the presence of IAV. It is unlikely that these proteins were released by active secretion, since *Spn* only has a Type II system that is used to transform DNA[100, 101], and there is no evidence suggesting that the Sec translocase pathway is involved in surface localization of the identified *Spn* proteins[102, 103]. Whether additional mechanisms exist to facilitate the release of *Spn* surface proteins, or if they are simply untethered from *Spn* surface due to capsule shedding, needs to be further studied. However, the significantly increased release of enolase, GAPDH, and PsaA that can facilitate plasminogen and complement binding and modulate host immune response suggests that capsule shedding is another strategy *Spn* uses to promote virulence upon contact with IAV. Of interest, while the majority of the proteomic changes caused by direct influenza virus were observed when infecting a system were epithelial cells were present, a set of bacterial proteins were further changed suggesting further adaptation as response to host signaling.

How pathogens adapt and tune their virulence in the polymicrobial environment is a fundamental question that needs to be addressed to truly understand pathogen behavior in the host. Pulmonary infections are commonly caused by respiratory pathogens including viruses and bacteria, and in many circumstances, a combination of both. Our results provide insights into the molecular mechanism behind the early stages of *Spn*-IAV pathogenic synergy. This may directly translate to bacterial synergism with SARS-CoV-2 viral infection[104, 105], providing another possible mechanism for development of severe infections. We foresee our results being directly

525 applicable to studies in other bacteria-virus interactions including other nasopharyngeal
526 commensals and pathogenic viruses.

527

528 ## Materials and Methods

529 **Bacterial and viral cultures**. *Spn* serotype 4 strain TIGR4 was grown overnight on 1% agar-
530 Todd Hewitt Broth (Thermo Fisher Scientific) with yeast (THY) plates supplemented with catalase.
531 Liquid cultures of THY were inoculated and grown to log-phase, then influenza A virus strain
532 Influenza A/Puerto Rico/8/1934 (PR8) was added (1:1 ratio) and incubated for 1 h. Selected
533 experiments used influenza A virus strain under the same conditions. *Spn* grown under the same
534 condition without added IAV served as control, and each experiment was performed with three
535 biological replicates. PR8 was propagated in embryonated chicken eggs[106, 107]. Stock viruses
536 were titered using plaque assays on MDCKs. IAV was heat-inactivated at 56°C for 30 min[108].
537 Growth curve was done by first growing *Spn* to log phase in THY, then seeded in a 96-well plate
538 at a volume of 100uL with/without IAV or heat-killed virus (HK IAV) and OD_{600} was measured
539 every 30 minutes. Transparent/opaque phenotype assessment was done as previously
540 described[98]. For experiments regarding the effects of glucose and galactose in the IAV-induced
541 bacterial changes, bacteria were grown in 50% THB with either 1% w/v glucose or galactose or
542 without sugar supplementation[109]. Bacterial cells were quantified upon growth in each medium
543 and diluted to an MOI of 10 for infection of A549 respiratory epithelial cells (ATCC). Adhesion and
544 invasion assays were done as previously described[98, 110]. For transcriptomics analysis TIGR4
545 was grown in CY media to around OD600=0.4. 100ul of PR8 stock at 10^8 TCID50/ml was added
546 to 10ml of TIGR4 cultures. For negative controls, 100ul of mock was added to 10ml of TIGR4
547 cultures. Cultures were incubated turning end-over-end at 37ºC for 15, 30, or 60 minutes. Each
548 time point and condition (virus/mock) was performed in triplicate. After incubation, cultures were

549 immediately spun down at 6,000xg and supernatant was discarded. Pellets were resuspended in
550 500ul RNAprotect Bacteria Reagent (QIAGEN, mat. 1018380) and frozen at -80°C. Isogenic
551 mutant deficient in ply were created by insertion of an erythromycin resistance cassette, ermB,
552 using allelic exchange, and grown in medium supplemented with 1 μg/ml of erythromycin as
553 previously described[111, 112]. Co-incubation model also include the use of *E. coli, P. aeruginosa*
554 and *S. marcescens*[22, 23] following the same protocol described above for *Spn*.

555 **Cell culture**. A549 type II alveolar epithelial cells were infected with IAV at MOI 2 for 4 hours, and
556 subsequently challenged with *Spn* at an MOI 10 for 4 hours as recently described[15].

557 **Immunoblots.** Samples for Western blotting were homogenized in PBS and sonicated, then
558 diluted in Laemmli buffer and aliquoted for storage at -80 degrees C. Samples were loaded into
559 4-15% gradient gels at 20 μg per lane, separated by SDS-PAGE, and transferred to nitrocellulose
560 membranes. Total protein was quantified by Ponceau stain, then membranes were blocked in
561 blocking buffer (TBS-0.01% Tween-20 containing 5% BSA) for at least 1 h. Primary antibodies
562 were diluted in blocking buffer and membranes were incubated overnight at 4 degrees C. Primary
563 antibodies used included: anti-pneumolysin antibody (ab71810, Abcam), anti-*Spn* serotype 4
564 (#16747, Statens Serum Institut) and cleaved-caspase-3 (AF835SP, R&D Systems) and β-actin
565 as loading control (ab8226, Abcam). HRP-tagged secondary antibodies were used to detect
566 primary antibodies (1:10,000 in blocking buffer) for 1 h. SuperSignal West PICO Plus
567 (ThermoFisher 34580) was used to develop HRP. All images were collected on an Amersham
568 Imager 680 (GE) and analyzed for densitometry in ImageJ. Briefly, to relatively quantify protein
569 bands from western blots relative to loading control (herein, total loaded protein).

570 **Capsule Shedding Assay.** TIGR4 bacteria was grown to OD600 0.5 in THY, washed once with
571 SMM buffer (0.5M sucrose, 0.02M MgCl2, 0.02M MES, pH 6.5), and resuspended in 1/10 volume
572 SMM buffer. Bacteria were incubated with IAV strains (MOI 1-0.001) or polymyxin B (32 mg/ml)

for 30 minutes at 37°C, then spun out at high speed. Supernatant was treated with proteinase K for 30 minutes at 37°C, then spotted on nitrocellulose membrane alongside serotype 4 capsular polysaccharide 3-6 μg (SSI Diagnostica cat. 76855). The membrane was then blocked with 5% BSA in TBS with 0.05% Tween-20 and probed overnight with anti-pneumococcus capsular antibody (1:500, SSI Diagnostica cat. 16747). Membranes were washed extensively, then probed with HRP-conjugated anti-rabbit secondary antibody and developed with Pierce ECL Western blotting substrate (ThermoFisher cat. 32109).

Cell lysate preparation, and protein digestion. The fresh cell pellets were first rinsed with cold PBS to remove culture medium contamination. The pellet fraction was then lysed with 2 x SED lysis buffer (4% SDS, 50mM EDTA, 20 mM DTT, 2% Tween 20, 100mM Tris-HCl, pH 8.0) followed by sonication (Misonix 3000, Ultrasonic Cell Disruptor) at amplitude 6 in six 30 s on/off cycles while cooling the lysates in an ice-water bath. After a 10 min centrifugation step at 16,000 × g, the soluble lysate fraction was collected. To estimate the protein concentration, an aliquot (10 ul) of each sample was analyzed on an SDS-PAGE gel alongside a known amount of BSA (2 μg)[113]. Proteins were digested following a Suspension Trapping (STrap) protocol with the self-packed glass fiber filters (Whatman, GF/F)[30]. After digestion, the resulting peptides were dried in a SpeedVac (Thermo Scientific) followed by C18-based desalting using StageTip protocol[114]. The peptides were lyophilized and then stored in -80°C until further analysis.

AE-MS procedure. Log-phase grown *Spn* (~1 × 10^{11} cells) were harvested, washed with PBS, and lysed by sonication in PBS containing HALT protease inhibitor cocktail (#78430, ThermoFisher). Clear lysate with soluble *Spn* proteins was obtained by centrifugation at high speed for 15 min, and half of it was mixed with 1 × 10^{8} IAV and 40 µL anti-HA agarose beads (Pierce cat. #26181) while the other half was directly mixed with anti-HA beads (control). Each group was performed in 3 replicate experiments. The mixing was performed overnight at 4°C with rotation. The next day, the beads were settled by centrifugation, the lysate was removed, and the

598 beads were washed extensively with PBS containing 0.05% Tween 20. Viral particles and *Spn*
599 proteins enriched on the beads were eluted by 5% SDS in 50 mM triethylammonium bicarbonate
600 (TEAB) and digested using the STrap method[30, 115]. After digestion, peptides were desalted
601 using the established StageTip method as descried above, and stored in -80ºC until further
602 analysis.

603 ***Spn* phosphopeptide enrichment.** Around 200 µg peptides resulted from STrap digestion of
604 *Spn* culture with or without IAV co-incubation were subjected to enrichment using titanium dioxide
605 beads according to the established protocol[57]. After enrichment, peptides were desalted using
606 StageTips before LC-MS/MS analysis.

607 ***Spn* conditioned media collection.** *Spn* was grown as described above to log-phase, then
608 incubated with IAV (or vehicle control) at a 1:1 ratio for 1 h at 37°C in quadruplicate. Cultures
609 were harvested by centrifugation at 9,000 × g for 15 min, and the supernatant was collected and
610 filtered through a 0.45 µm disc filter. Proteins in the supernatant were concentrated by Amicon
611 Ultra-15 filter (10K MWCO) and buffer exchanged into 50 mM ammonium bicarbonate by
612 centrifugation. Concentrated proteins were collected and mixed with 4% SDS and 25 mM DTT,
613 then digested using the STrap method as described above. Conditioned media was also used for
614 macrophage phagocytosis assay (using MH-S cells)[21, 116] and complement hemolysis assays
615 (using sheep red blood cells) [117].

616 **LC-MS/MS analysis**. The LC-MS/MS analysis was conducted on an Ultimate 3000 RSLCnano
617 System coupled to a quadrupole Orbitrap mass spectrometer (Q Exactive, Thermo Scientific) via
618 a nano electrospray ion source. The experimental methods were described previously in
619 detail[118] In brief, the desalted peptide samples were first dissolved into 20 µl LC buffer A (0.1%
620 formic acid in water), and then loaded onto a PepMap C18 trap column (100 µm x 2 cm, 5 µm
621 particle size, Thermo Scientific) followed by separation on an in-house packed column (75 mm x

622 19 cm, 3.0 mm ReproSil-Pur C18-AQ). Depending on sample complexity, we utilized varied LC
623 gradient to maximize the identification rate and throughput. For the host cell (A549) related
624 experiment, a 220-min gradient (180 min from 2% to 35% buffer B, 0.1% formic acid in acetonitrile;
625 10 min to 80% B) was used. For the samples from pulldown assay, phosphorylation enrichment,
626 and Spn/Flu experiment, a 150-min gradient (120 min from 2% to 35% buffer B, 0.1% formic acid
627 in acetonitrile; 10 min to 80% B) was used. The full (MS1) scans were acquired at a resolution of
628 70,000 with a mass range of *m/z* 300-1,700 in a data-dependent mode. The ten most intense ions
629 were selected from each cycle for MS/MS (MS2) analysis using high-energy collisional
630 dissociation (HCD) with normalized collision energy of 27%. The dynamic exclusion time was set
631 to 20 seconds. Singly charged ions and ions with five or more charges were excluded for MS/MS
632 analysis. The MS2 scans were performed at a resolution of 17,500. Target value for the full scan
633 MS scan was 5×10^5 with a maximum injection time of 20 ms, and for MS/MS scan was 1×10^6
634 with a maximum injection time of 100 ms.

635 **Protein identification and quantitation**. The MS raw data were searched against a meta
636 database that contained protein sequences of *Streptococcus pneumoniae* serotype 4 (strain
637 ATCC BAA-334 / TIGR4) (UniProt taxon identifier 170187; 2,115 sequences), Influenza A virus
638 (strain A/Puerto Rico/8/1934 H1N1) (UniProt taxon identifier 211044; 112 sequences) and Homo
639 sapiens (UniProt taxon identifier 9606; 17,023 reviewed sequences). To determine proteins
640 associated with culture media additional searches for Canis Lupus familiaris (UniProt taxon
641 identifier 9615), Bos taurus (UniProt taxon identifier 9913) and Sus scrofa domesticus (UniProt
642 taxon identifier 9825) were performed. The MaxQuant-Andromeda software suite (version
643 1.6.5.0) was employed with most of the default settings[119]. Two mis-cleavage sites were
644 allowed; the minimum peptide length was set to seven amino acids. Protein N-terminal acetylation
645 and oxidation (M) and were set as variable modifications; carbamidomethylation (C) was set as
646 fixed modification. The MS1 and MS2 ion tolerances were set at 20 ppm and 10 ppm, respectively.

The false-discovery rate (FDR) of 1% was set at both peptide and protein level. The embedded label-free algorithm (MaxLFQ) was enabled using a minimum ratio count of 1. Further bioinformatics analyses such as Hierarchical clustering, Principal Component Analysis (PCA), t-tests, volcano plots and correlation analyses were performed in Perseus software (version 1.6.7.0)[120]. The LFQ data were first log2 transformed and then filtered to include those that were present in at least two of the three biological replicates in one of the two groups. The missing values were imputed based on default parameters. For hierarchical clustering, the Z-scored LFQ intensities were used with Euclidean as a distance measure for both column and row clustering.

RNA Extraction. TIGR4 samples were thawed and pelleted at 6,000xg for 10 minutes. Supernatant was discarded. Pellets were resuspended in 400µl of RLT Lysis Buffer (QIAGEN mat. 1015762). 10µl of 2-Mercaptoethanol had been added to the RLT buffer for every 1 ml buffer. All 400µl samples were loaded into Lysing Matrix E tubes (MP Biomedicals, ref. 6914100). Samples were lysed with the Fast Prep-24 (MP Biomedicals) homogenizer for 10 pulses, 20 seconds each. All samples were incubated at 70°C for 10 minutes or until clear. Lysate was spun through QIA Shredder columns (QIAGEN, cat. 79656) for 1 min at max speed. Flow-through was returned to the column and spun again for a total of three spins. Samples were combined with 400µl of 70% ethanol and loaded onto RNeasy mini columns (QIAGEN RNeasy Mini Kit, cat. 74104). RNA was extracted following the RNeasy protocol, eluting in 70µl of nuclease-free water. RNA sample concentrations were measured by Nanodrop. RNA-quality was assessed by the Hartwell Center for Biotechnology at St. Jude Research Hospital.

DNA Removal. For each TIGR4 RNA sample, 10µg RNA was combined with 1µl rDNAse I from the DNA Removal Kit (Thermo Scientific cat. AM1906). A tenth of the total volume of 10X DNase I buffer was added to each sample. Samples were incubated at 37°C for 30 minutes. 2µl DNase Inactivation Reagent was added to each sample. Samples were incubated at RT for 2 minutes.

671 Samples were spun at 10,000xg for 90 seconds. Supernatant was transferred and measured by
672 Nanodrop.

673 **Ribosomal RNA Depletion**. The ribosomal RNA depletion protocol was adapted from Culviner
674 et al. 2020[121]. Biotinylated primers were combined into a mix to pull down rRNA. The mix
675 contained 10µl of each 5S primer and 5µl of the remaining primers. Primers started at the stock
676 concentration of 100µM. 2X Binding/Wash (B&W) buffer was made to contain 10 mM 7.6 pH Tris,
677 1mM EDTA, and 2M NaCl. For each 10 samples, Dynabeads™ MyOne™ Streptavidin C1 beads
678 (Thermo Scientific, cat. 65002) were prepared by pulling down 1.41ml beads with a magnetic
679 rack. Beads were washed 3 times with 1.5ml 1X B&W buffer before being resuspended in 300µl
680 2X B&W. 10µl SUPERase-IN™ RNase Inhibitor (Thermo Scientific, cat. AM2696) was added to
681 each batch. 30µl of prepared beads were used for each sample. Each sample mix received 3µl
682 20X SSC, 1µl 30mM EDTA, 1µl diluted oligo mix, 3µg of RNA sample, and water up to 30µl in a
683 PCR tube. Samples were incubated at 70°C for 5 min in a thermocycler, stepping down a degree
684 every 30 seconds down to 25°C. Samples were combined with the 30µl of beads and were
685 thoroughly mixed. Tubes were incubated for 5 minutes RT, vortexed, and incubated again for 5
686 minutes at 50°C. Beads were pulled down by magnet and supernatant was transferred to new
687 tubes. Each sample received 140µl water, 20µl 3M NaOAc pH 5.5, 2µl GlycoBlue™ (Thermo
688 Scientific, cat. AM9516), and 600µl pure ethanol. Samples were kept at -20°C. Samples were
689 spun at 14,000xg at 4°C for 30 minutes. Supernatant was removed; pellets were washed with
690 800µl cold 70% ethanol. Samples were spun at 14,000xg for 5 minutes at 4°C. Supernatant was
691 discarded; pellets were resuspended in 10µl nuclease-free water and stored at -20°C. Used
692 primers are shown in **Table S2**.

693 **Generating cDNA.** NEB Next Ultra II RNA Library Prep Kit for Illumina (#E7775) was used to
694 generate cDNA from 5µl RNA sample according to the provided protocol using the random primer
695 method. Products were purified with Agencourt AMPure XP beads (Beckman Coulter Product No.

A63881). 144µl resuspended beads were added to 80µl product, incubating at RT for 5 minutes. Beads were pulled down by magnet, supernatant was removed. Beads were washed twice with 200µl 80% ethanol. Beads were left at RT to dry 5 minutes before eluting with 53µl TE. 50µl supernatant was transferred to new plate.

Adaptor Ligation. NEB Next Ultra II RNA Library Prep Kit for Illumina was used to ligate adaptors to 50µl samples of cDNA. Products were purified by AMPure XP beads as previously described, eluting in 17µl 0.1X TE. 15µl supernatant was transferred to a new plate. PCR enrichment for adaptor ligated DNA was also performed using NEB Next Ultra II RNA Library Prep Kit for Illumina. AMPure XP beads were used to purify PCR products, eluting in 23 µl 0.1XTE, transferring 20µl to another plate for sequencing.

Sequencing. The library was prepped using the TruSeq Stranded Total RNA by Illumina (PN. 20020597). Samples were sequenced on the Illumina Novaseq 6000.

RNA-seq analysis. Raw paired-end reads in FASTQ format were processed by fastp v0.20.0 to remove adaptor sequences, short reads (length < 20) and low quality reads with a Phred quality score < 25. The resulting clean reads were aligned against the respective *Spn* reference genomes (TIGR4: NC_003028.3, D39: NC_008533.2, BHN97x: CP025076.1) using bowtie2 (version 2.3.5) based on different experimental designs. SAM/BAM files were processed by Samtools 0.1.19. The featureCounts v2.0.1 from the Subread package was used to count mapped reads for genes with a MAPQ value ≥ 10. Raw read counts were first normalized by variance stabilizing transformation by DESeq2, and then differential gene expression analysis was carried out by DESeq2 (log2-fold ≥1 and adjusted p-values ≤0.05). Heatmaps and volcano plots were generated to visualize statistically significant genes by pheatmap (1.0.12) and EnhancedVolcano (1.4.0), respectively, in R version 3.6.3.

Data considerations and statistics. Unless otherwise noted, all *in vitro* experiments are composed of a minimum of 3 biological replicates, with ≥3 technical replicates each. Statistical comparisons were calculated using GraphPad Prism 8 (La Jolla, CA). Comparisons between two cohorts at a single time point are calculated by Mann-Whitney U test. Comparisons between groups of >2 cohorts or groups given multiple treatments were calculated by ANOVA with Tukey's (one-way) or Sidak's (two-way) post-test or by Kruskal-Wallis H test with Dunn's multiple comparison post-test, as determined by the normality of data groups. Repeated measures are accounted for whenever applicable.

Data Sharing. The mass spectrometry proteomics data have been deposited to the ProteomeXchange Consortium via the PRIDE partner repository with the dataset identifier PXD016214 and PXD016122. The raw RNA-seq data has been deposited to NCBI database under the accession number PRJNA837613.

References

1. Rolfes MA, Foppa IM, Garg S, Flannery B, Brammer L, Singleton JA, Burns E, Jernigan D, Olsen SJ, Bresee J *et al*: **Annual estimates of the burden of seasonal influenza in the United States: A tool for strengthening influenza surveillance and preparedness**. *Influenza Other Respir Viruses* 2018, **12**(1):132-137.

2. Torner N, Navas E, Soldevila N, Toledo D, Navarro G, Morillo A, Perez MJ, Dominguez A, Working Group of the Project PI: **Costs associated with influenza-related hospitalization in the elderly**. *Hum Vaccin Immunother* 2017, **13**(2):412-416.

3. Centers for Disease C, Prevention: **Bacterial coinfections in lung tissue specimens from fatal cases of 2009 pandemic influenza A (H1N1) - United States, May-August 2009**. *MMWR Morb Mortal Wkly Rep* 2009, **58**(38):1071-1074.

4. Ampofo K, Herbener A, Blaschke AJ, Heyrend C, Poritz M, Korgenski K, Rolfs R, Jain S, Carvalho Mda G, Pimenta FC *et al*: **Association of 2009 pandemic influenza A (H1N1) infection and increased hospitalization with parapneumonic empyema in children in Utah**. *Pediatr Infect Dis J* 2010, **29**(10):905-909.

5. Almand EA, Moore MD, Jaykus L-A: **Virus-Bacteria Interactions: An Emerging Topic in Human Infection**. *Viruses* 2017, **9**(3):58.

6. Morris DE, Cleary DW, Clarke SC: **Secondary Bacterial Infections Associated with Influenza Pandemics**. *Frontiers in microbiology* 2017, **8**:1041-1041.

7. Jain S, Self WH, Wunderink RG, Fakhran S, Balk R, Bramley AM, Reed C, Grijalva CG, Anderson EJ, Courtney DM *et al*: **Community-Acquired Pneumonia Requiring Hospitalization among U.S. Adults**. *N Engl J Med* 2015, **373**(5):415-427.

8. Marks LR, Davidson BA, Knight PR, Hakansson AP: **Interkingdom signaling induces Streptococcus pneumoniae biofilm dispersion and transition from asymptomatic colonization to disease**. *mBio* 2013, **4**(4):e00438-00413.

9. Smith EL, Wheeler I, Adler H, Ferreira DM, Sa-Leao R, Abdullahi O, Adetifa I, Becker-Dreps S, Esposito S, Farida H *et al*: **Upper airways colonisation of Streptococcus pneumoniae in adults aged 60 years and older: A systematic review of prevalence and individual participant data meta-analysis of risk factors**. *J Infect* 2020, **81**(4):540-548.

10. McCullers JA: **The co-pathogenesis of influenza viruses with bacteria in the lung**. *Nat Rev Microbiol* 2014, **12**(4):252-262.

11. McCullers JA, Bartmess KC: **Role of neuraminidase in lethal synergism between influenza virus and Streptococcus pneumoniae**. *J Infect Dis* 2003, **187**(6):1000-1009.

12. McCullers JA, English BK: **Improving therapeutic strategies for secondary bacterial pneumonia following influenza**. *Future Microbiol* 2008, **3**(4):397-404.

13. McCullers JA: **Insights into the interaction between influenza virus and pneumococcus**. *Clinical microbiology reviews* 2006, **19**(3):571-582.

14. Shi Z, Gewirtz AT: **Together Forever: Bacterial-Viral Interactions in Infection and Immunity**. *Viruses* 2018, **10**(3):122.

15. Gonzalez-Juarbe N, Riegler AN, Jureka AS, Gilley RP, Brand JD, Trombley JE, Scott NR, Platt MP, Dube PH, Petit CM *et al*: **Influenza-Induced Oxidative Stress Sensitizes Lung Cells to Bacterial-Toxin-Mediated Necroptosis**. *Cell Rep* 2020, **32**(8):108062.

16. Smith AM, McCullers JA: **Secondary bacterial infections in influenza virus infection pathogenesis**. *Curr Top Microbiol Immunol* 2014, **385**:327-356.

17. Pettigrew MM, Marks LR, Kong Y, Gent JF, Roche-Hakansson H, Hakansson AP: **Dynamic changes in the Streptococcus pneumoniae transcriptome during transition from biofilm formation to invasive disease upon influenza A virus infection**. *Infection and immunity* 2014, **82**(11):4607-4619.

781 18. Rowe HM, Meliopoulos VA, Iverson A, Bomme P, Schultz-Cherry S, Rosch JW: **Direct**
782 **interactions with influenza promote bacterial adherence during respiratory**
783 **infections**. *Nature Microbiology* 2019, **4**(8):1328-1336.
784 19. Smith CM, Sandrini S, Datta S, Freestone P, Shafeeq S, Radhakrishnan P, Williams G,
785 Glenn SM, Kuipers OP, Hirst RA *et al*: **Respiratory syncytial virus increases the**
786 **virulence of Streptococcus pneumoniae by binding to penicillin binding protein**
787 **1a. A new paradigm in respiratory infection**. *Am J Respir Crit Care Med* 2014,
788 **190**(2):196-207.
789 20. Hament JM, Aerts PC, Fleer A, van Dijk H, Harmsen T, Kimpen JL, Wolfs TF: **Direct**
790 **binding of respiratory syncytial virus to pneumococci: a phenomenon that**
791 **enhances both pneumococcal adherence to human epithelial cells and**
792 **pneumococcal invasiveness in a murine model**. *Pediatr Res* 2005, **58**(6):1198-1203.
793 21. Park SS, Gonzalez-Juarbe N, Riegler AN, Im H, Hale Y, Platt MP, Croney C, Briles DE,
794 Orihuela CJ: **Streptococcus pneumoniae binds to host GAPDH on dying lung**
795 **epithelial cells worsening secondary infection following influenza**. *Cell Rep* 2021,
796 **35**(11):109267.
797 22. Gonzalez-Juarbe N, Gilley RP, Hinojosa CA, Bradley KM, Kamei A, Gao G, Dube PH,
798 Bergman MA, Orihuela CJ: **Pore-Forming Toxins Induce Macrophage Necroptosis**
799 **during Acute Bacterial Pneumonia**. *PLoS Pathog* 2015, **11**(12):e1005337.
800 23. Gonzalez-Juarbe N, Mares CA, Hinojosa CA, Medina JL, Cantwell A, Dube PH, Orihuela
801 CJ, Bergman MA: **Requirement for Serratia marcescens cytolysin in a murine**
802 **model of hemorrhagic pneumonia**. *Infect Immun* 2015, **83**(2):614-624.
803 24. Weiser JN, Austrian R, Sreenivasan PK, Masure HR: **Phase variation in**
804 **pneumococcal opacity: relationship between colonial morphology and**
805 **nasopharyngeal colonization**. *Infect Immun* 1994, **62**(6):2582-2589.

25. Keilhauer EC, Hein MY, Mann M: **Accurate Protein Complex Retrieval by Affinity Enrichment Mass Spectrometry (AE-MS) Rather than Affinity Purification Mass Spectrometry (AP-MS)**. *Molecular & Cellular Proteomics* 2015, **14**(1):120-135.

26. Kadioglu A, Weiser JN, Paton JC, Andrew PW: **The role of Streptococcus pneumoniae virulence factors in host respiratory colonization and disease**. *Nature Reviews Microbiology* 2008, **6**(4):288-301.

27. Tilley SJ, Orlova EV, Gilbert RJC, Andrew PW, Saibil HR: **Structural Basis of Pore Formation by the Bacterial Toxin Pneumolysin**. *Cell* 2005, **121**(2):247-256.

28. Ramachandran R, Tweten RK, Johnson AE: **Membrane-dependent conformational changes initiate cholesterol-dependent cytolysin oligomerization and intersubunit β-strand alignment**. *Nature Structural & Molecular Biology* 2004, **11**(8):697-705.

29. Price KE, Camilli A: **Pneumolysin Localizes to the Cell Wall of Streptococcus pneumoniae**. *Journal of Bacteriology* 2009, **191**(7):2163-2168.

30. Lin Y-H, Eguez RV, Torralba MG, Singh H, Golusinski P, Golusinski W, Masternak M, Nelson KE, Freire M, Yu Y: **Self-Assembled STrap for Global Proteomics and Salivary Biomarker Discovery**. *Journal of Proteome Research* 2019, **18**(4):1907-1915.

31. Cox J, Hein MY, Luber CA, Paron I, Nagaraj N, Mann M: **Accurate Proteome-wide Label-free Quantification by Delayed Normalization and Maximal Peptide Ratio Extraction, Termed MaxLFQ**. *Mol Cell Proteomics* 2014, **13**(9):2513-2526.

32. Hoyer J, Bartel J, Gomez-Mejia A, Rohde M, Hirschfeld C, Hess N, Sura T, Maass S, Hammerschmidt S, Becher D: **Proteomic response of Streptococcus pneumoniae to iron limitation**. *Int J Med Microbiol* 2018, **308**(6):713-721.

33. Kilstrup M, Hammer K, Ruhdal Jensen P, Martinussen J: **Nucleotide metabolism and its control in lactic acid bacteria**. *FEMS Microbiology Reviews* 2005, **29**(3):555-590.

34. García E, López R: **Molecular biology of the capsular genes of Streptococcus pneumoniae**. *FEMS Microbiology Letters* 2006, **149**(1):1-10.

832 35. Hardy GG, Caimano MJ, Yother J: **Capsule Biosynthesis and Basic Metabolism**
833 **inStreptococcus pneumoniae Are Linked through the Cellular**
834 **Phosphoglucomutase**. *Journal of Bacteriology* 2000, **182**(7):1854-1863.
835 36. Okura M, Takamatsu D, Maruyama F, Nozawa T, Nakagawa I, Osaki M, Sekizaki T,
836 Gottschalk M, Kumagai Y, Hamada S: **Genetic analysis of capsular polysaccharide**
837 **synthesis gene clusters from all serotypes of Streptococcus suis: potential**
838 **mechanisms for generation of capsular variation**. *Applied and environmental*
839 *microbiology* 2013, **79**(8):2796-2806.
840 37. Bajaj R, Bruce KE, Davidson AL, Rued BE, Stauffacher CV, Winkler Malcolm E:
841 **Biochemical characterization of essential cell division proteins FtsX and FtsE that**
842 **mediate peptidoglycan hydrolysis by PcsB in Streptococcus pneumoniae**.
843 *MicrobiologyOpen* 2016, **5**(5):738-752.
844 38. Mura A, Fadda D, Perez AJ, Danforth ML, Musu D, Rico AI, Krupka M, Denapaite D,
845 Tsui H-CT, Winkler ME *et al*: **Roles of the Essential Protein FtsA in Cell Growth and**
846 **Division in <span class="named-content genus-species" id="named-content-**
847 **1">Streptococcus pneumoniae**. *Journal of Bacteriology* 2017, **199**(3):e00608-
848 00616.
849 39. Zapun A, Vernet T, Pinho MG: **The different shapes of cocci**. *FEMS Microbiology*
850 *Reviews* 2008, **32**(2):345-360.
851 40. Al-Bayati FAY, Kahya HFH, Damianou A, Shafeeq S, Kuipers OP, Andrew PW,
852 Yesilkaya H: **Pneumococcal galactose catabolism is controlled by multiple**
853 **regulators acting on pyruvate formate lyase**. *Scientific Reports* 2017, **7**(1):43587.
854 41. Shelburne SA, Keith D, Horstmann N, Sumby P, Davenport MT, Graviss EA, Brennan
855 RG, Musser JM: **A direct link between carbohydrate utilization and virulence in the**
856 **major human pathogen group A Streptococcus**. *Proceedings of the*
857 *National Academy of Sciences* 2008, **105**(5):1698-1703.

858 42. Carvalho SM, Kloosterman TG, Kuipers OP, Neves AR: **CcpA Ensures Optimal**
859 **Metabolic Fitness of Streptococcus pneumoniae**. *PLOS ONE* 2011, **6**(10):e26707.
860 43. Abranches J, Nascimento MM, Zeng L, Browngardt CM, Wen ZT, Rivera MF, Burne RA:
861 **CcpA regulates central metabolism and virulence gene expression in**
862 **Streptococcus mutans**. *Journal of bacteriology* 2008, **190**(7):2340-2349.
863 44. Paixão L, Oliveira J, Veríssimo A, Vinga S, Lourenço EC, Ventura MR, Kjos M, Veening
864 J-W, Fernandes VE, Andrew PW *et al*: **Host glycan sugar-specific pathways in**
865 **Streptococcus pneumoniae: galactose as a key sugar in colonisation and**
866 **infection [corrected]**. *PloS one* 2015, **10**(3):e0121042-e0121042.
867 45. Zeng L, Das S, Burne RA: **Utilization of Lactose and Galactose by**
868 **Streptococcus mutans: Transport, Toxicity, and Carbon Catabolite**
869 **Repression**. *Journal of Bacteriology* 2010, **192**(9):2434-2444.
870 46. Tan M-F, Gao T, Liu W-Q, Zhang C-Y, Yang X, Zhu J-W, Teng M-Y, Li L, Zhou R:
871 **MsmK, an ATPase, Contributes to Utilization of Multiple Carbohydrates and Host**
872 **Colonization of Streptococcus suis**. *PloS one* 2015, **10**(7):e0130792-e0130792.
873 47. Marion C, Aten AE, Woodiga SA, King SJ: **Identification of an ATPase, MsmK, Which**
874 **Energizes Multiple Carbohydrate ABC Transporters in <span class="named-**
875 **content genus-species" id="named-content-1">Streptococcus**
876 **pneumoniae**. *Infection and Immunity* 2011, **79**(10):4193-4200.
877 48. Shaper M, Hollingshead SK, Benjamin WH, Jr., Briles DE: **PspA protects**
878 **Streptococcus pneumoniae from killing by apolactoferrin, and antibody to PspA**
879 **enhances killing of pneumococci by apolactoferrin [corrected]**. *Infection and*
880 *immunity* 2004, **72**(9):5031-5040.
881 49. Jeremy Brown SHaCO: **Streptococcus Pneumoniae: Molecular Mechanisms of**
882 **Host-Pathogen Interactions**. 2015.

50. Lindsey R. Burcham RAH, Rachel C. Caulkins, Joseph P. Emerson, Bindu Nanduri, Jason W. Rosch, Nicholas C. Fitzkee, Justin A. Thornton: **SP1433-1438 operon of Streptococcus pneumoniae regulates metal homeostasis and cellular metabolism during zinc-stress**. *bioRxiv 367086; doi: https://doiorg/101101/367086* 2018.

51. Orihuela CJ, Radin JN, Sublett JE, Gao G, Kaushal D, Tuomanen EI: **Microarray analysis of pneumococcal gene expression during invasive disease**. *Infect Immun* 2004, **72**(10):5582-5596.

52. Ubersax JA, Ferrell JE, Jr.: **Mechanisms of specificity in protein phosphorylation**. *Nat Rev Mol Cell Biol* 2007, **8**(7):530-541.

53. Beilharz K, Nováková L, Fadda D, Branny P, Massidda O, Veening J-W: **Control of cell division in Streptococcus pneumoniae by the conserved Ser/Thr protein kinase StkP**. *Proceedings of the National Academy of Sciences* 2012, **109**(15):E905-E913.

54. Potel CM, Lin MH, Heck AJR, Lemeer S: **Widespread bacterial protein histidine phosphorylation revealed by mass spectrometry-based proteomics**. *Nat Methods* 2018, **15**(3):187-190.

55. Nourikyan J, Kjos M, Mercy C, Cluzel C, Morlot C, Noirot-Gros M-F, Guiral S, Lavergne J-P, Veening J-W, Grangeasse C: **Autophosphorylation of the Bacterial Tyrosine-Kinase CpsD Connects Capsule Synthesis with the Cell Cycle in Streptococcus pneumoniae**. *PLOS Genetics* 2015, **11**(9):e1005518.

56. Humphrey SJ, Azimifar SB, Mann M: **High-throughput phosphoproteomics reveals in vivo insulin signaling dynamics**. *Nature Biotechnology* 2015, **33**(9):990.

57. Thingholm TE, Jørgensen TJD, Jensen ON, Larsen MR: **Highly selective enrichment of phosphorylated peptides using titanium dioxide**. *Nature Protocols* 2006, **1**(4):1929-1935.

58. Olsen JV, Blagoev B, Gnad F, Macek B, Kumar C, Mortensen P, Mann M: **Global, in vivo, and site-specific phosphorylation dynamics in signaling networks**. *Cell* 2006, **127**(3):635-648.

59. Sun X, Ge F, Xiao C-L, Yin X-F, Ge R, Zhang L-H, He Q-Y: **Phosphoproteomic Analysis Reveals the Multiple Roles of Phosphorylation in Pathogenic Bacterium Streptococcus pneumoniae**. *Journal of Proteome Research* 2010, **9**(1):275-282.

60. Manuse S, Fleurie A, Zucchini L, Lesterlin C, Grangeasse C: **Role of eukaryotic-like serine/threonine kinases in bacterial cell division and morphogenesis**. *FEMS Microbiology Reviews* 2015, **40**(1):41-56.

61. Grangeasse C: **Rewiring the Pneumococcal Cell Cycle with Serine/Threonine- and Tyrosine-kinases**. *Trends in Microbiology* 2016, **24**(9):713-724.

62. Fleurie A, Manuse S, Zhao C, Campo N, Cluzel C, Lavergne J-P, Freton C, Combet C, Guiral S, Soufi B *et al*: **Interplay of the serine/threonine-kinase StkP and the paralogs DivIVA and GpsB in pneumococcal cell elongation and division**. *PLoS genetics* 2014, **10**(4):e1004275-e1004275.

63. Nováková L, Bezousková S, Pompach P, Spidlová P, Sasková L, Weiser J, Branny P: **Identification of multiple substrates of the StkP Ser/Thr protein kinase in Streptococcus pneumoniae**. *Journal of bacteriology* 2010, **192**(14):3629-3638.

64. Hirschfeld C, Gómez-Mejia A, Bartel J, Hentschker C, Rohde M, Maaß S, Hammerschmidt S, Becher D: **Proteomic Investigation Uncovers Potential Targets and Target Sites of Pneumococcal Serine-Threonine Kinase StkP and Phosphatase PhpP**. *Frontiers in Microbiology* 2020, **10**(3101).

65. Fleurie A, Cluzel C, Guiral S, Freton C, Galisson F, Zanella-Cleon I, Di Guilmi A-M, Grangeasse C: **Mutational dissection of the S/T-kinase StkP reveals crucial roles in cell division of Streptococcus pneumoniae**. *Molecular Microbiology* 2012, **83**(4):746-758.

66. Rued BE, Zheng JJ, Mura A, Tsui H-CT, Boersma MJ, Mazny JL, Corona F, Perez AJ, Fadda D, Doubravová L *et al*: **Suppression and synthetic-lethal genetic relationships of ΔgpsB mutations indicate that GpsB mediates protein phosphorylation and penicillin-binding protein interactions in Streptococcus pneumoniae D39**. *Molecular microbiology* 2017, **103**(6):931-957.

67. Gunnewijk MGW, Poolman B: **Phosphorylation State of HPr Determines the Level of Expression and the Extent of Phosphorylation of the Lactose Transport Protein ofStreptococcus thermophilus**. *Journal of Biological Chemistry* 2000, **275**(44):34073-34079.

68. Hoskins J, Alborn WE, Arnold J, Blaszczak LC, Burgett S, DeHoff BS, Estrem ST, Fritz L, Fu D-J, Fuller W *et al*: **Genome of the Bacterium Streptococcus pneumoniae Strain R6**. *Journal of Bacteriology* 2001, **183**(19):5709-5717.

69. Brooks LRK, Mias GI: **Streptococcus pneumoniae's Virulence and Host Immunity: Aging, Diagnostics, and Prevention**. *Frontiers in Immunology* 2018, **9**(1366).

70. Huberts DHEW, van der Klei IJ: **Moonlighting proteins: An intriguing mode of multitasking**. *Biochimica et Biophysica Acta (BBA) - Molecular Cell Research* 2010, **1803**(4):520-525.

71. Kolberg J, Aase A, Bergmann S, Herstad TK, Rodal G, Frank R, Rohde M, Hammerschmidt S: **Streptococcus pneumoniae enolase is important for plasminogen binding despite low abundance of enolase protein on the bacterial cell surface**. *Microbiology (Reading)* 2006, **152**(Pt 5):1307-1317.

72. Bergmann S, Rohde M, Chhatwal GS, Hammerschmidt S: **α-Enolase of Streptococcus pneumoniae is a plasmin(ogen)-binding protein displayed on the bacterial cell surface**. *Molecular Microbiology* 2001, **40**(6):1273-1287.

957 73. Díaz-Ramos A, Roig-Borrellas A, García-Melero A, López-Alemany R: **α-Enolase, a**
958 **multifunctional protein: its role on pathophysiological situations**. *Journal of*
959 *biomedicine & biotechnology* 2012, **2012**:156795-156795.
960 74. Bergmann S, Rohde M, Hammerschmidt S: **Glyceraldehyde-3-phosphate**
961 **dehydrogenase of Streptococcus pneumoniae is a surface-displayed**
962 **plasminogen-binding protein**. *Infection and immunity* 2004, **72**(4):2416-2419.
963 75. Agarwal V, Hammerschmidt S, Malm S, Bergmann S, Riesbeck K, Blom AM: **Enolase of**
964 **Streptococcus pneumoniae Binds Human Complement Inhibitor C4b-**
965 **Binding Protein and Contributes to Complement Evasion**. *The Journal of*
966 *Immunology* 2012, **189**(7):3575-3584.
967 76. Terrasse R, Tacnet-Delorme P, Moriscot C, Pérard J, Schoehn G, Vernet T, Thielens
968 NM, Di Guilmi AM, Frachet P: **Human and Pneumococcal Cell Surface**
969 **Glyceraldehyde-3-phosphate Dehydrogenase (GAPDH) Proteins Are Both Ligands**
970 **of Human C1q Protein**. *Journal of Biological Chemistry* 2012, **287**(51):42620-42633.
971 77. Rajam G, Anderton JM, Carlone GM, Sampson JS, Ades EW: **Pneumococcal Surface**
972 **Adhesin A (PsaA): A Review**. *Critical Reviews in Microbiology* 2008, **34**(3-4):131-142.
973 78. Johnston JW, Myers LE, Ochs MM, Benjamin WH, Jr., Briles DE, Hollingshead SK:
974 **Lipoprotein PsaA in virulence of Streptococcus pneumoniae: surface accessibility**
975 **and role in protection from superoxide**. *Infection and immunity* 2004, **72**(10):5858-
976 5867.
977 79. Tseng H-J, McEwan AG, Paton JC, Jennings MP: **Virulence of Streptococcus**
978 **pneumoniae: PsaA Mutants Are Hypersensitive to Oxidative Stress**. *Infection*
979 *and Immunity* 2002, **70**(3):1635-1639.
980 80. Wilkins JC, Beighton D, Homer KA: **Effect of acidic pH on expression of surface-**
981 **associated proteins of Streptococcus oralis**. *Applied and environmental microbiology*
982 2003, **69**(9):5290-5296.

983 81. Mohan S, Hertweck C, Dudda A, Hammerschmidt S, Skerka C, Hallström T, Zipfel PF:
984 **Tuf of Streptococcus pneumoniae is a surface displayed human complement**
985 **regulator binding protein**. *Molecular Immunology* 2014, **62**(1):249-264.
986 82. Nishimoto AT, Rosch JW, Tuomanen EI: **Pneumolysin: Pathogenesis and**
987 **Therapeutic Target**. *Front Microbiol* 2020, **11**:1543.
988 83. Kietzman CC, Gao G, Mann B, Myers L, Tuomanen EI: **Dynamic capsule**
989 **restructuring by the main pneumococcal autolysin LytA in response to the**
990 **epithelium**. *Nat Commun* 2016, **7**:10859.
991 84. Ferraris RP, Yasharpour S, Lloyd KC, Mirzayan R, Diamond JM: **Luminal glucose**
992 **concentrations in the gut under normal conditions**. *Am J Physiol* 1990, **259**(5 Pt
993 1):G822-837.
994 85. Krismer B, Liebeke M, Janek D, Nega M, Rautenberg M, Hornig G, Unger C,
995 Weidenmaier C, Lalk M, Peschel A: **Nutrient limitation governs Staphylococcus**
996 **aureus metabolism and niche adaptation in the human nose**. *PLoS Pathog* 2014,
997 **10**(1):e1003862.
998 86. Lorin MI, Gaerlan PF, Mandel ID: **Quantitative composition of nasal secretions in**
999 **normal subjects**. *J Lab Clin Med* 1972, **80**(2):275-281.
1000 87. Vanthanouvong V, Roomans GM: **Methods for determining the composition of nasal**
1001 **fluid by X-ray microanalysis**. *Microsc Res Tech* 2004, **63**(2):122-128.
1002 88. Rowe HM, Meliopoulos VA, Iverson A, Bomme P, Schultz-Cherry S, Rosch JW: **Direct**
1003 **interactions with influenza promote bacterial adherence during respiratory**
1004 **infections**. *Nat Microbiol* 2019, **4**(8):1328-1336.
1005 89. Eschapasse E, Hussenet C, Bergeron A, Lebeaux D: **[Respiratory infections caused**
1006 **by slow-growing bacteria: Nocardia, Actinomyces, Rhodococcus]**. *Rev Mal Respir*
1007 2017, **34**(6):661-671.

1008 90. Cozens RM, Tuomanen E, Tosch W, Zak O, Suter J, Tomasz A: **Evaluation of the**
1009 **bactericidal activity of beta-lactam antibiotics on slowly growing bacteria cultured**
1010 **in the chemostat**. *Antimicrob Agents Chemother* 1986, **29**(5):797-802.
1011 91. Maria-Neto S, de Almeida KC, Macedo ML, Franco OL: **Understanding bacterial**
1012 **resistance to antimicrobial peptides: From the surface to deep inside**. *Biochim*
1013 *Biophys Acta* 2015, **1848**(11 Pt B):3078-3088.
1014 92. Al-Bayati FA, Kahya HF, Damianou A, Shafeeq S, Kuipers OP, Andrew PW, Yesilkaya
1015 H: **Pneumococcal galactose catabolism is controlled by multiple regulators acting**
1016 **on pyruvate formate lyase**. *Sci Rep* 2017, **7**:43587.
1017 93. Gilley RP, Orihuela CJ: **Pneumococci in biofilms are non-invasive: implications on**
1018 **nasopharyngeal colonization**. *Front Cell Infect Microbiol* 2014, **4**:163.
1019 94. Wolf AI, Strauman MC, Mozdzanowska K, Williams KL, Osborne LC, Shen H, Liu Q,
1020 Garlick D, Artis D, Hensley SE *et al*: **Pneumolysin expression by streptococcus**
1021 **pneumoniae protects colonized mice from influenza virus-induced disease**.
1022 *Virology* 2014, **462-463**:254-265.
1023 95. Hakansson A, Roche H, Mirza S, McDaniel LS, Brooks-Walter A, Briles DE:
1024 **Characterization of binding of human lactoferrin to pneumococcal surface protein**
1025 **A**. *Infect Immun* 2001, **69**(5):3372-3381.
1026 96. Beiter K, Wartha F, Hurwitz R, Normark S, Zychlinsky A, Henriques-Normark B: **The**
1027 **capsule sensitizes Streptococcus pneumoniae to alpha-defensins human**
1028 **neutrophil proteins 1 to 3**. *Infection and immunity* 2008, **76**(8):3710-3716.
1029 97. Bradshaw JL, McDaniel LS: **Selective pressure: Rise of the nonencapsulated**
1030 **pneumococcus**. *PLoS Pathog* 2019, **15**(8):e1007911.
1031 98. Shenoy AT, Brissac T, Gilley RP, Kumar N, Wang Y, Gonzalez-Juarbe N, Hinkle WS,
1032 Daugherty SC, Shetty AC, Ott S *et al*: **Streptococcus pneumoniae in the heart**

subvert the host response through biofilm-mediated resident macrophage killing. *PLoS Pathog* 2017, **13**(8):e1006582.

99. Park IH, Kim K-H, Andrade AL, Briles DE, McDaniel LS, Nahm MH: **Nontypeable Pneumococci Can Be Divided into Multiple cps Types, Including One Type Expressing the Novel Gene pspK**. *mBio* 2012, **3**(3):e00035-00012.

100. Laurenceau R, Péhau-Arnaudet G, Baconnais S, Gault J, Malosse C, Dujeancourt A, Campo N, Chamot-Rooke J, Le Cam E, Claverys J-P *et al*: **A Type IV Pilus Mediates DNA Binding during Natural Transformation in Streptococcus pneumoniae**. *PLOS Pathogens* 2013, **9**(6):e1003473.

101. Balaban M, Bättig P, Muschiol S, Tirier SM, Wartha F, Normark S, Henriques-Normark B: **Secretion of a pneumococcal type II secretion system pilus correlates with DNA uptake during transformation**. *Proceedings of the National Academy of Sciences* 2014, **111**(7):E758-E765.

102. Tsui H-CT, Keen SK, Sham L-T, Wayne KJ, Winkler ME: **Dynamic distribution of the SecA and SecY translocase subunits and septal localization of the HtrA surface chaperone/protease during Streptococcus pneumoniae D39 cell division**. *mBio* 2011, **2**(5):e00202-00211.

103. Bandara M, Skehel JM, Kadioglu A, Collinson I, Nobbs AH, Blocker AJ, Jenkinson HF: **The accessory Sec system (SecY2A2) in Streptococcus pneumoniae is involved in export of pneumolysin toxin, adhesion and biofilm formation**. *Microbes and Infection* 2017, **19**(7):402-412.

104. Huang C, Wang Y, Li X, Ren L, Zhao J, Hu Y, Zhang L, Fan G, Xu J, Gu X *et al*: **Clinical features of patients infected with 2019 novel coronavirus in Wuhan, China**. *Lancet* 2020, **395**(10223):497-506.

105. Kim D, Quinn J, Pinsky B, Shah NH, Brown I: **Rates of Co-infection Between SARS-CoV-2 and Other Respiratory Pathogens**. *JAMA* 2020, **323**(20):2085-2086.

106. Brauer R, Chen P: **Influenza virus propagation in embryonated chicken eggs**. *J Vis Exp* 2015(97).

107. Spackman E, Killian ML: **Avian influenza virus isolation, propagation, and titration in embryonated chicken eggs**. *Methods Mol Biol* 2014, **1161**:125-140.

108. Zou S, Guo J, Gao R, Dong L, Zhou J, Zhang Y, Dong J, Bo H, Qin K, Shu Y: **Inactivation of the novel avian influenza A (H7N9) virus under physical conditions or chemical agents treatment**. *Virol J* 2013, **10**:289.

109. Blanchette-Cain K, Hinojosa CA, Akula Suresh Babu R, Lizcano A, Gonzalez-Juarbe N, Munoz-Almagro C, Sanchez CJ, Bergman MA, Orihuela CJ: **Streptococcus pneumoniae biofilm formation is strain dependent, multifactorial, and associated with reduced invasiveness and immunoreactivity during colonization**. *MBio* 2013, **4**(5):e00745-00713.

110. Kharat AS, Tomasz A: **Inactivation of the srtA gene affects localization of surface proteins and decreases adhesion of Streptococcus pneumoniae to human pharyngeal cells in vitro**. *Infect Immun* 2003, **71**(5):2758-2765.

111. Lizcano A, Chin T, Sauer K, Tuomanen EI, Orihuela CJ: **Early biofilm formation on microtiter plates is not correlated with the invasive disease potential of Streptococcus pneumoniae**. *Microb Pathog* 2010, **48**(3-4):124-130.

112. Shivshankar P, Sanchez C, Rose LF, Orihuela CJ: **The Streptococcus pneumoniae adhesin PsrP binds to Keratin 10 on lung cells**. *Mol Microbiol* 2009, **73**(4):663-679.

113. Yu Y, Suh MJ, Sikorski P, Kwon K, Nelson KE, Pieper R: **Urine sample preparation in 96-well filter plates for quantitative clinical proteomics**. *Anal Chem* 2014, **86**(11):5470-5477.

114. Yu Y, Pieper R: **Using Proteomics to Identify Inflammation During Urinary Tract Infection**. *Methods Mol Biol* 2019, **2021**:259-272.

115. HaileMariam M, Eguez RV, Singh H, Bekele S, Ameni G, Pieper R, Yu Y: **S-Trap, an Ultrafast Sample-Preparation Approach for Shotgun Proteomics**. *J Proteome Res* 2018, **17**(9):2917-2924.

116. Mina MJ, Brown LA, Klugman KP: **Dynamics of Increasing IFN-gamma Exposure on Murine MH-S Cell-Line Alveolar Macrophage Phagocytosis of Streptococcus pneumoniae**. *J Interferon Cytokine Res* 2015, **35**(6):474-479.

117. Inglis JE, Radziwon KA, Maniero GD: **The serum complement system: a simplified laboratory exercise to measure the activity of an important component of the immune system**. *Adv Physiol Educ* 2008, **32**(4):317-321.

118. Lin YH, Platt MP, Fu H, Gui Y, Wang Y, Gonzalez-Juarbe N, Zhou D, Yu Y: **Global proteome and phosphoproteome characterization of sepsis-induced kidney injury**. *Mol Cell Proteomics* 2020.

119. Tyanova S, Temu T, Cox J: **The MaxQuant computational platform for mass spectrometry-based shotgun proteomics**. *Nat Protocols* 2016, **11**(12):2301-2319.

120. Tyanova S, Cox J: **Perseus: A Bioinformatics Platform for Integrative Analysis of Proteomics Data in Cancer Research**. In: *Cancer Systems Biology: Methods and Protocols.* Edited by von Stechow L. New York, NY: Springer New York; 2018: 133-148.

121. Culviner PH, Guegler CK, Laub MT: **A Simple, Cost-Effective, and Robust Method for rRNA Depletion in RNA-Sequencing Studies**. *mBio* 2020, **11**(2).

Declarations

Ethics approval and consent to participate. Not applicable

Consent for publication. Not applicable

Availability of data and materials. The datasets generated and/or analyzed during the current study are available from the corresponding author on reasonable request.

Competing Interests. We declare that none of the authors have competing financial or non-financial interests.

Funding. N.G-J. was supported in part by the National Institutes for Health (NIH) awards AI148722-01A1, ES030227 and J. Craig Venter Institute Start-Up Funds. This study was also supported in part by the National Cancer Institute of the NIH under Award Number P30 CA021765 and 1R56AI155614-01A1 to J.W.R.

Author Contributions. M.P.P., Y-H.L., T.P., I.V., R.W-R, and Y.Y. carried out the experiments, M.P.P., Y-H.L., Y.Y. J.W.R. and N.G.J contributed to the design and conceptualization of the project. M.P.P., Y-H.L., C.A.M., J.W.R., Y.Y. and N.G.J wrote and edited the manuscript.

Acknowledgements. Not applicable